

1
2
3
4
5
6
7
8
9
10
11

Air-water CO₂ evasion from U.S. East Coast estuaries

Goossens, Nicolas¹, Laruelle, Goulven Gildas^{1*}, Arndt, Sandra², Cai, Wei-Jun³ & Regnier, Pierre¹

1 Department Geosciences, Environment and Society, Université Libre de Bruxelles, Brussels, Belgium

2 School of Geographical Sciences, University of Bristol, Bristol, UK

3 School of Marine Science and Policy, University of Delaware, Newark, Delaware, USA

*corresponding author: goulven.gildas.laruelle@ulb.ac.be

12 **Abstract:**

13 This study presents the first regional-scale assessment of estuarine CO₂ evasion along the East coast
14 of the US (25 – 45 °N). The focus is on 43 tidal estuaries, which together drain a catchment of
15 697000 km² or 76 % of the total area within this latitudinal band. The approach is based on the
16 Carbon – Generic Estuarine Model (C-GEM) that allows simulating hydrodynamics, transport and
17 biogeochemistry for a wide range of estuarine systems using readily available geometric parameters
18 and global databases of seasonal climatic, hydraulic, and riverine biogeochemical information. Our
19 simulations, performed using conditions representative of the year 2000, suggest that, together, US
20 East coast estuaries emit 1.9 TgC yr⁻¹ in the form of CO₂, which correspond to about 40 % of the
21 carbon inputs from rivers, marshes and mangroves. Carbon removal within estuaries results from a
22 combination of physical (outgassing of supersaturated riverine waters) and biogeochemical
23 processes (net heterotrophy and nitrification). The CO₂ evasion and its underlying drivers show
24 important variations across individual systems, but reveal a clear latitudinal pattern characterized by
25 a decrease in the relative importance of physical over biogeochemical processes along a North-South
26 gradient. Finally, the results reveal that the ratio of estuarine surface area to the river discharge, S/Q
27 (which has a scale of per meter discharged water per year), could be used as a predictor of the
28 estuarine carbon processing in future regional and global scale assessments.

29 **1 Introduction**

30 Carbon fluxes along the land-ocean aquatic continuum are currently receiving increasing attention
31 because of their recently recognized role in the global carbon cycle and anthropogenic CO₂ budget
32 (Bauer et al., 2013; Regnier et al., 2013a; LeQuéré et al., 2014, 2015). Estuaries are important
33 reactive conduits along this continuum, which links the terrestrial and marine global carbon cycles
34 (Cai, 2011). Large amounts of terrestrial carbon transit through these systems, where they mix with
35 carbon from autochthonous, as well as marine sources. During estuarine transit, heterotrophic
36 processes degrade a fraction of the allochthonous and autochthonous organic carbon inputs,
37 supporting a potentially significant, yet poorly quantified CO₂ evasion flux to the atmosphere. Recent
38 estimates suggest that 0.15-0.25 PgC yr⁻¹ is emitted from estuarine systems worldwide (Borges and
39 Abril, 2012; Cai, 2011; Laruelle et al., 2010; Regnier et al., 2013a; Laruelle et al., 2013, Bauer et al.,
40 2013). Thus, in absolute terms the global estuarine CO₂ evasion corresponds to about 15% of the
41 open ocean CO₂ uptake despite the much smaller total surface area.

42 Currently, estimates of regional and global estuarine CO₂ emissions are mainly derived on the basis
43 of data-driven approaches that rely on the extrapolation of a small number of local measurements
44 (Cai, 2011; Chen et al., 2013; Laruelle et al., 2013). These approaches fail to capture the spatial and
45 temporal heterogeneity of the estuarine environment (Bauer et al., 2013) and are biased towards
46 anthropogenically influenced estuarine systems located in industrialized countries (Regnier et al.,
47 2013a). Even in the best surveyed regions of the world (e.g. Australia, Western Europe, North
48 America or China) observations are merely available for a small number of estuarine systems. In
49 addition, if available, data sets are generally of low spatial and temporal resolution. As a
50 consequence, data-driven approaches can only provide first-order estimates of regional and global
51 estuarine CO₂ emissions.

52 Integrated model-data approaches can help here, as models provide the means to extrapolate over
53 temporal and spatial scales and allow disentangling the complex and very dynamic network of

54 physical and biogeochemical processes that controls estuarine CO₂ emissions. Over the past
55 decades, increasingly complex process-based models have been applied, in combination with local
56 data, to elucidate the coupled carbon-nutrient cycles on the scale of individual estuaries (e.g.,
57 O’Kane, 1980; Soetaert and Herman, 1995; Vanderborght et al., 2002; Lin et al., 2007; Arndt et al.,
58 2009; Cerco et al., 2010; Baklouti et al., 2011). However, the application of such model approaches
59 remains limited to the local scale due to their high data requirements for calibration and validation
60 (e.g. bathymetric and geometric information and boundary conditions), as well as the high
61 computational demand associated with resolving the complex interplay of physical and
62 biogeochemical processes on the relevant temporal and spatial scales (Regnier et al., 2013b).
63 Complex process-based models are thus not suitable for the application on a regional or global scale
64 and, as a consequence, the estuarine carbon filter is, despite its increasingly recognized role in
65 regional and global carbon cycling (e.g. Bauer et al., 2013), typically not taken into account in model-
66 derived regional or global carbon budgets (Bauer et al., 2013). The lack of regional and global model
67 approaches that could be used as stand-alone applications or that could be coupled to regional
68 terrestrial river network models (e.g. GLOBALNEWS: Seitzinger et al., 2005; Mayorga et al., 2010;
69 SPARROW: Schwarz et al., 2006) and continental shelf models (e.g. Hofmann et al., 2011) is thus
70 critical.

71 The Carbon-Generic Estuary Model (C-GEM (v1.0); Volta et al., 2014) has been developed with the
72 aim of providing such a regional/global modeling tool that can help improve existing, observationally
73 derived first order estimates of estuarine CO₂ emissions. C-GEM (v1.0) has been specifically designed
74 to reduce data requirements and computational demand and, thus, tackles the main impediments
75 for the application of estuarine models on a regional or global scale. The approach takes advantage
76 of the mutual dependency between estuarine geometry and hydrodynamics in alluvial estuaries
77 and uses an idealized representation of the estuarine geometry to support the hydrodynamic
78 calculations. It thus allows running steady state or fully transient annual to multi-decadal simulations
79 for a large number of estuarine systems, using geometric information readily available through maps

80 or remote sensing images. Although the development of such a regional/global tool inevitably
81 requires simplification, careful model evaluations have shown that, despite the geometric
82 simplification, C-GEM provides an accurate description of the hydrodynamics, transport and
83 biogeochemistry in tidal estuaries (Volta et al., 2014). In addition, the model approach was
84 successfully used to quantify the contribution of different biogeochemical processes for CO₂ air-
85 water fluxes in an idealized, funnel-shaped estuary forced by typical summer conditions
86 characterizing a temperate Western European climate (Regnier et al., 2013b). Volta et al. (2016b)
87 further investigated the effect of estuarine geometry on the CO₂ outgassing using three idealized
88 systems and subsequently established the first regional carbon budget for estuaries surrounding the
89 North Sea by explicitly simulating the six largest systems of the area (Volta et al., 2016a), including
90 the Scheldt and the Elbe for which detailed validation was performed.

91 Here, we extend the domain of application of C-GEM (v1.0) to quantify CO₂ exchange fluxes, as well
92 as the overall organic and inorganic carbon budgets for the full suite of estuarine systems located
93 along the entire East coast of the United States, one of the most intensively monitored regions in the
94 world. A unique set of regional data, including partial pressure of CO₂ in riverine and continental
95 shelf waters (pCO₂; Signorini et al., 2013; Laruelle et al., 2015), riverine biogeochemical
96 characteristics (Lauerwald et al., 2013), estuarine eutrophication status (Bricker et al., 2007) and
97 estuarine morphology (NOAA, 1985) are available. These comprehensive data sets are
98 complemented by local observations of carbon cycling and CO₂ fluxes in selected, individual
99 estuarine systems (see Laruelle et al., 2013 for a review), making the East coast of the United States
100 an ideal region for a first, fully explicit regional evaluation of CO₂ evasion resolving every major tidal
101 estuary along the selected coastal segment. The scale addressed in the present study is
102 unprecedented so far (> 3000 km of coastline) and covers a wide range of estuarine morphological
103 features, climatic conditions, land-use and land cover types, as well as urbanization levels. The
104 presented study will not only allow a further evaluation of C-GEM (v1.0), but will also provide the
105 first regional-scale assessment of estuarine CO₂ evasion along the East coast of the US (25 – 45 °N)

106 and will help explore general relationships between carbon cycling and CO₂ evasion, and readily
107 available estuarine geometrical parameters.

108 After a description of the model itself and of the dataset used to set up the simulations, a local
109 validation is presented which includes salinity, pCO₂ and pH longitudinal profiles for two well
110 monitored systems (the Delaware Bay and the Altamaha River Estuary). The yearly averaged rates of
111 CO₂ exchange at the air-water interface simulated by the model for 13 individual estuaries are also
112 compared with observed values reported in the literature. Next, regional scale simulations for 43
113 tidal estuaries of the eastern US coast provide seasonal and yearly integrated estimates of the Net
114 Ecosystem Metabolism (NEM), CO₂ evasion and carbon filtering capacity, CFilt. Model results are
115 then used to elucidate the estuarine biogeochemical behavior along the latitudinal transect
116 encompassed by the present study (30-45° N). Finally, our results are used to derive general
117 relationships between carbon cycling and CO₂ evasion, and readily available estuarine geometrical
118 parameters.

119

120 **2. Regional description and model approach**

121 **2.1 Observation-based carbon budget for the East coast of the United States**

122 The study area covers the Atlantic coast of the United States (Fig.1), from the southern tip of Florida
123 (25°N) to Cobscook Bay (45°N) at the US-Canada boundary. This area encompasses distinct climatic
124 zones and land cover types and exhibits a variety of morphologic features (Fig. 1). The region can be
125 subdivided into several sub-regions following a latitudinal gradient (Signorini et al., 2013). In this
126 study, we define three sub-regions following the boundaries suggested by the COSCAT segmentation
127 (Meybeck et al., 2006; Laruelle et al., 2013) and the further subdivision described in Laruelle et al.
128 (2015). From North to South, the regions are called North Atlantic, Mid Atlantic and South Atlantic
129 Regions (Fig. 1). Total carbon inputs from watersheds to US East coast estuaries (Tab. 1) have been

130 estimated to range from 4.0 to 10.7 Tg C yr⁻¹ (Mayorga et al., 2010; Shih et al., 2010; Stets and Strieg,
131 2012; Tian et al., 2010; Tian et al., 2012), consisting of dissolved organic carbon (DOC; ~50%),
132 dissolved inorganic carbon (DIC; ~40%) and particulate organic carbon (POC; ~10%). In addition, a
133 statistical approach has been applied to estuaries of the region to quantify organic carbon budgets
134 and Net Ecosystem Productivity (NEP) using empirical models (Herrmann et al., 2015).

135 Recent studies estimated that, along the East coast of the United States, rivers emit 11.4 TgC yr⁻¹ of
136 CO₂ to the atmosphere (Raymond et al., 2013), while continental shelf waters absorb between 3.4
137 and 5.4 TgC yr⁻¹ of CO₂ from the atmosphere (Signorini et al., 2013). A total of thirteen local, annual
138 mean estuarine CO₂ flux estimates across the air-water interface based on measurements are also
139 reported in the literature and are grouped along a latitudinal gradient (Tab. 2). Four of these
140 estimates are located in the South Atlantic region (SAR): Sapelo Sound, Doboy Sound, Altamaha
141 Sound (Jiang et al., 2008), and the Satilla River estuary (Cai and Wang, 1998). Three studies
142 investigate CO₂ fluxes in the mid-Atlantic Region (MAR): the York River Estuary (Raymond et al.,
143 2000) and the Hudson River (Raymond et al., 1997). There is also a comprehensive CO₂ flux study for
144 the Delaware Estuary published after the completion of this work (Joeseof et al., 2015). Six systems
145 are located in the North Atlantic region (NAR): The Great Bay, the Little Bay, the Oyster estuary, the
146 Bellamy estuary, the Cocheco estuary (Hunt et al., 2010; 2011), and the Parker River estuary
147 (Raymond and Hopkinson, 2003). The mean annual flux per unit area from these local studies is
148 11.7±13.1 mol C m⁻² yr⁻¹ and its extrapolation to the total estuarine surface leads to a regional CO₂
149 evasion estimate of 3.8 Tg C yr⁻¹. This estimate is in line with that of Laruelle et al. (2013) for the same
150 region which proposes an average CO₂ emission rate of 10.8 mol C m⁻² yr⁻¹. Thus, CO₂ outgassing
151 could remove 35% to 95% of the riverine carbon loads during estuarine transit. About 75 % of the
152 air-water exchange occurs in tidal estuaries (2.8 Tg C yr⁻¹) while lagoons and small deltas contribute to
153 the remaining 25 %. Although these simple extrapolations from limited observational data are
154 associated with large uncertainties, they highlight the potentially significant contribution of estuaries
155 to the CO₂ outgassing in the region. However, process-based quantifications of regional organic and

156 inorganic C budgets including air-water CO₂ fluxes for the estuarine systems along the East coast are
157 not available.

158 **2.2 Selection of estuaries**

159 The National Estuarine Eutrophication Assessment (NEEA) survey (Bricker et al., 2007), which uses
160 geospatial data from the National Oceanic and Atmospheric Administration (NOAA) Coastal
161 Assessment Framework (CAF) (NOAA, 1985), was used to identify and characterize 58 estuarine
162 systems discharging along the Atlantic coast of the United States. From this set, 43 'tidal' estuaries,
163 defined as a river stretch of water that is tidally influenced (Dürr et al., 2011), were retained (Fig. 1)
164 to be simulated by the C-GEM model, which is designed to represent such systems. Using outputs
165 from terrestrial models (Hartmann et al., 2009; Mayorga et al., 2010), the cumulated riverine carbon
166 loads for all the non-tidal estuaries that are excluded from the present study amount to 0.9 Tg C yr⁻¹,
167 which represents less than 15% of the total riverine carbon loads of the region. These 15 systems are
168 located in the SAR (10) and in the MAR (5).

169 The northeastern part of the domain (NAR, Fig. 1; Tab. 1) includes 20 estuaries along the Gulf of
170 Maine and the Scotian shelf, covering a cumulative surface area of ~5300 km². It includes drowned
171 valleys, rocky shores and a few tidal marshes. The climate is relatively cold (annual mean= 8°C) and
172 the human influence is relatively limited because of low population density and low freshwater
173 inputs. The mean estuarine water depth is 12.9 m and the mean tidal range is 2.8 m.

174 The central zone (MAR) includes 17 tidal estuaries accounting for a total surface area of 14500 km².
175 The Chesapeake Bay and the Delaware estuaries alone contribute more than 60% to the surface area
176 of the region. In this region, estuaries are drowned valleys with comparatively high river discharge
177 and intense exchange with the ocean. Several coastal lagoons, characterized by a limited exchange
178 with the ocean are located here, but are not included in our analysis. The Mid-Atlantic Region (MAR)
179 is characterized by a mean annual temperature of 13°C and is strongly impacted by human activities,

180 due to the presence of several large cities (e.g. New York, Washington, Philadelphia, Baltimore) and
181 intense agriculture. The mean water depth is about 4.7 m and the tidal range is 0.8 m.

182 The southern Atlantic region (SAR) includes 10 tidal estuaries covering a total surface area of 12182
183 km². These systems are generally dendritic and surrounded by extensive salt marshes. The climate is
184 subtropical with an average annual temperature of 19°C. Land use includes agriculture and industry,
185 but the population density is generally low. Estuarine systems in the SAR are characterized by a
186 shallow mean water depth of 2.9 m and a tidal range of 1.2 m.

187 **2.3 Model set-up**

188 The generic 1D Reactive-Transport Model (RTM) C-GEM (Volta et al., 2014) is used to quantify the
189 estuarine carbon cycling in the 43 systems considered in this study. The approach is based on
190 idealized geometries (Savenije, 2005; Volta et al., 2014) and is designed for regional and global scale
191 applications (Regnier et al., 2013b; Volta et al., 2014, 2016a). The model approach builds on the
192 premise that hydrodynamics exerts a first-order control on estuarine biogeochemistry (Arndt et al.,
193 2007; Friedrichs and Hofmann, 2001) and CO₂ fluxes (Regnier et al., 2013a). The method takes
194 advantage of the mutual dependence between geometry and hydrodynamics in tidal estuaries
195 (Savenije, 1992) and the fact that, as a consequence, transport and mixing can be easily quantified
196 from readily available geometric data (Regnier et al., 2013a; Savenije, 2005; Volta et al., 2016b).

197 **2.3.1 Description of idealized geometries for tidally-averaged conditions**

198 Although tidal estuaries display a wide variety of shapes, they nevertheless share common
199 geometric characteristics that are compatible with an idealized representation (Fig. 2, Savenije,
200 1986; Savenije, 2005). For tidally-averaged conditions, their width B (or cross-sectional area A) can
201 be described by an exponential decrease as a function of distance, x , from the mouth (Savenije,
202 1986; Savenije, 2005):

$$B = B_0 * \exp\left(-\frac{x}{b}\right) \quad (1)$$

203 where B (m) is the tidally averaged width, B₀ (m) the width at the mouth, x (m) the distance from
 204 the mouth (x=0) and b (m) the width convergence length (Fig. 2). The width convergence length, b, is
 205 defined as the distance between the mouth and the point at which the width is reduced to B₀ e⁻¹. It
 206 is directly related to the dominant hydrodynamic forcing. A high river discharge typically results in a
 207 prismatic channel with long convergence length (river dominated estuary), while a large tidal range
 208 results in a funnel-shaped estuary with short convergence length (marine dominated estuary). At the
 209 upstream boundary, the estuarine width is given by:

$$B_L = B_0 * \exp\left(-\frac{L}{b}\right) \quad (2)$$

210 Where L denotes the total estuarine length (m) along the estuarine longitudinal axis.

211 The total estuarine surface S (m²) can be estimated by integrating equation (1) over the estuarine
 212 length:

$$S = \int_0^L B dx = b * B_0 * \left(1 - \exp\left(-\frac{L}{b}\right)\right) \quad (3)$$

213

214 The width convergence length is then calculated from B₀, B_L, L and the real estuarine surface area
 215 (SR) by inserting equation (2) in equation (3):

$$b = \frac{SR}{B_0 - B_L} \quad (4)$$

216 SR is calculated for each system using the SRTM water body data (Fig. 3a), a geographical dataset
 217 encoding high-resolution worldwide coastal outlines in a vector format (NASA/NGA, 2003). While
 218 such a database exists for a well monitored region such as the East coast of the US, resorting to
 219 using the idealized estuarine surface area (S) is necessary in many other regions. The longitudinal

220 mean, tidally averaged, depth h (m), is obtained from the National Estuarine Eutrophication
 221 Assessment database (Bricker et al., 2007).

222 Using this idealized representation, the estuarine geometry can be defined by a limited number of
 223 parameters: the width at the mouth (B_0), the estuarine length (L), the estuarine width at the
 224 upstream limit (B_L) and the mean depth h . These parameters can be easily determined from local
 225 maps or Google Earth using Geographic Information Systems (GIS) or obtained from databases
 226 (NASA/NGA, 2003).

227 2.3.2 Hydrodynamics, transport and biogeochemistry

228 Estuarine hydrodynamics are described by the one-dimensional barotropic, cross-sectionally
 229 integrated mass and momentum conservation equations for a channel with arbitrary geometry
 230 (Nihoul and Ronday, 1976; Regnier et al., 1998; Regnier and Steefel, 1999):

$$231 \quad r_s \frac{\partial A}{\partial t} + \frac{\partial Q}{\partial x} = 0 \quad (5)$$

$$232 \quad \frac{\partial U}{\partial t} + U \frac{\partial U}{\partial x} = -g \frac{\partial \zeta}{\partial x} - g \frac{U|U|}{C_H^2 H} \quad (6)$$

233 where:

234	t	time	[s]
235	x	distance along the longitudinal axis	[m]
236	A	cross-section area $A = H \cdot B$	[m ²]
237	Q	cross-sectional discharge $Q = A \cdot U$	[m ³ s ⁻¹]
238	U	flow velocity Q/A	[m s ⁻¹]
239	r_s	storage ratio $r_s = B_s/B$	[-]

240	B_s	storage width	[m]
241	g	gravitational acceleration	[m s ⁻²]
242	ξ	elevation	[m]
243	H	total water depth $H = h + \xi(x, t)$	[m]
244	C_z	Chézy coefficient	[m ^{1/2} s ⁻¹]

245 The coupled partial differential equations (Eqs. (5) and (6)) are solved by specifying the elevation
 246 $\xi_0(t)$ at the estuarine mouth and the river discharge $Q_r(t)$ at the upstream limit of the model domain.

247 The one-dimensional, tidally-resolved, advection-dispersion equation for a constituent of
 248 concentration $C(x, t)$ in an estuary can be written as (e.g. Pritchard, 1958):

$$249 \quad \frac{\partial C}{\partial t} + \frac{Q}{A} \frac{\partial C}{\partial x} = \frac{1}{A} \frac{\partial}{\partial x} \left(AD \frac{\partial C}{\partial x} \right) + P \quad (7)$$

250 where $Q(x, t)$ and $A(x, t)$ denote the cross-sectional discharge and area, respectively and are provided
 251 by the hydrodynamic model (eq. 5 and 6). $P(x, t)$ is the sum of all production and consumption
 252 process rates affection the concentration of the constituent. The effective dispersion coefficient D
 253 (m² s⁻¹) implicitly accounts for dispersion mechanisms associated to sub-grid scale processes (Fischer,
 254 1976; Regnier et al., 1998). In general, D is maximal near the sea, decreases upstream and becomes
 255 virtually zero near the tail of the salt intrusion curve (Preddy, 1954; Kent, 1958; Ippen and Harleman,
 256 1961; Stigter and Siemons, 1967). The effective dispersion at the estuarine mouth can be quantified
 257 by the following relation (Savenije, 1986):

$$258 \quad D_0 = 26 \cdot (h_0)^{1.5} \cdot (N \cdot g)^{0.5} \quad (8)$$

259 where h_0 (m) is the tidally-averaged water depth at the estuarine mouth and N is the dimensionless
 260 Canter Cremers' estuary number defined as the ratio of the freshwater entering the estuary during a

261 tidal cycle to the volume of salt water entering the estuary over a tidal cycle (Simmons, 1955).

$$262 \quad N = \frac{Q_b \cdot T}{P} \quad (9)$$

263 In this equation, Q_b is the bankfull discharge ($\text{m}^3 \text{s}^{-1}$), T is the tidal period (s) and P is the tidal prism
264 (m^3). For each estuary, N can thus be calculated directly from the hydrodynamic model. The
265 variation in D along the estuarine gradient can be described by Van der Burgh's equation (Savenije,
266 1986):

$$267 \quad \frac{\partial D}{\partial x} = -K \frac{Q_r}{A} \quad (10)$$

268 where K is the dimensionless Van der Burgh's coefficient and the minus sign indicates that D
269 increases in downstream direction (Savenije, 2012). The Van der Burgh's coefficient is a shape factor
270 that has values between 0 and 1 (Savenije, 2012), and is a function of estuarine geometry for tidally
271 average conditions. Therefore, each estuarine system has its own characteristic K value, which
272 correlates with geometric and hydraulic scales (Savenije, 2005). Based on a regression analysis
273 covering a set of 15 estuaries, it has been proposed to constrain K from the estuarine geometry
274 (Savenije, 1992):

$$275 \quad K = 4.32 \cdot \frac{h_0^{0.36}}{B_0^{0.21} \cdot b^{0.14}} \quad \text{with } 0 < K < 1 \quad (11)$$

276 Reaction processes P considered in C-GEM comprise aerobic degradation, denitrification,
277 nitrification, primary production, phytoplankton mortality and air-water gas exchange for O_2 and CO_2
278 (Fig. 4 and Tab. 3). These processes and their mathematical formulation are described in detail in
279 Volta et al. (2014) and Volta et al. (2016a).

280 The non-linear partial differential equations for the hydrodynamics are solved by a finite difference
281 scheme following the approach of (Regnier et al., 1997; Regnier and Steefel, 1999) and
282 (Vanderborgh et al., 2002). The timestep Δt is 150s and the grid size Δx is constant along the

283 longitudinal axis of the estuary. The grid size default value is 2000 m, but can be smaller for short
284 length estuaries to guarantee a minimum of 20 grid points within the computational domain.
285 Transport and reaction terms are solved in sequence within a single timestep using an operator
286 splitting approach (Regnier et al., 1997). The advection term in the transport equation is integrated
287 using a third-order accurate total variation diminishing (TVD) algorithm with flux limiters (Regnier et
288 al., 1998), ensuring monotonicity (Leonard, 1984), while a semi-implicit Crank-Nicholson algorithm is
289 used for the dispersion term (Press et al., 1992). These schemes have been extensively tested using
290 the CONTRASTE estuarine model (e.g. Regnier et al., 1998; Regnier and Steefel, 1999; Vanderborght
291 et al., 2002) and guarantee mass conservation to within <1%. The reaction network (including
292 erosion-deposition terms when the constituent is a solid species), is numerically integrated using the
293 Euler method (Press et al., 1992). The primary production dynamics, which requires vertical
294 resolution of the photic depth, is calculated according to the method described in Vanderborght et
295 al. (2007). This method assumes an exponential decrease of the light in the water column (Platt et
296 al., 1980), which is solved using a Gamma function.

297 **2.4 Boundary and forcing conditions**

298 Boundary and forcing conditions are extracted from global databases and global model outputs that
299 are available at 0.5° resolution. Therefore, C-GEM simulations are performed at the same resolution
300 according to the following procedure. First, 43 coastal cells corresponding to tidal estuaries are
301 identified in the studied area (Fig. 1). If the mouth of an estuary is spread over several 0.5° grid cells,
302 those cells are regrouped in order to represent a single estuary (e.g. Delaware estuary), and
303 subsequently, a single idealized geometry is defined as described above. The model outputs
304 (Hartmann et al. , 2009; Mayorga et al., 2010) and databases (Antonov et al., 2010; Garcia et al.,
305 2010a; Garcia et al., 2010b) used to constrain our boundary conditions are representative of the
306 year 2000.

307 For each resulting cell, boundary and forcing conditions are calculated for the following periods:
308 January-March; April-June; July-September and October-December. This allows for an explicit
309 representation of the seasonal variability in the simulations.

310 **2.4.1 External forcings**

311 Transient physical forcings are calculated for each season and grid cell using monthly mean values of
312 water temperature (World Ocean Atlas, 2009) and seasonal averaged values for wind speed (Cross-
313 Calibrated-Multi-Platform (CCMP) Ocean Surface Wind Vector Analyses project (Atlas et al., 2011)).
314 Mean daily solar radiation and photoperiods (corrected for cloud coverage using the ISCCP Cloud
315 Data Products, Rossow and Schiffer, 1999) are calculated depending on latitude and day of the year
316 using a simple model (Brock, 1981).

317 **2.4.2 Riverine discharge, concentrations and fluxes**

318 River discharges are extracted from the UNH/GRDC runoff dataset (Fekete et al., 2002). These
319 discharges represent long-term averages (1960-1990) of monthly and annual runoff at 0.5 degree
320 resolution. The dataset is a composite of long-term gauging data, which provides average runoff for
321 the largest river basins, and a climate driven water balance model (Fekete et al., 2002). Total runoff
322 values are then aggregated for each watershed at the coarser 0.5 degree resolution (Fig. 3b). Next,
323 seasonal mean values (in $\text{m}^3 \text{s}^{-1}$) are derived in order to account for the intra-annual variability in
324 water fluxes. Based on annual carbon and nutrients inputs from the watersheds ($\text{Mg} \text{y}^{-1}$), mean
325 annual concentrations ($\text{mmol} \text{m}^{-3}$) are estimated for each watershed using the UNH/GRDC annual
326 runoff ($\text{km}^3 \text{y}^{-1}$). Mean seasonal concentrations are then calculated from the seasonally resolved
327 river water fluxes of a given sub-region.

328 Annual inputs of dissolved organic carbon (DOC), particulate organic carbon (POC) and inorganic
329 nutrients are derived from the globalNEWS2 model (Mayorga et al., 2010). Global NEWS is a spatially
330 explicit, multi-element (N, P, Si, C) and multi-form global model of nutrient exports by rivers. In a

331 nutshell, DOC exports are a function of runoff, wetland area, and consumptive water use (Harrison
332 et al., 2005). No distinction is made between agricultural and natural landscapes, since they appear
333 to have similar DOC export coefficients (Harrison et al., 2005). Sewage inputs of OC are ignored in
334 GlobalNEWS, because their inclusion did not improve model fit to data (Harrison et al., 2005). POC
335 exports from watersheds are estimated using an empirical relationship with Suspended Particulate
336 Matter (SPM; Ludwig et al., 1996). Inorganic nitrogen (DIN) and phosphorus (DIP) fluxes calculated
337 by GlobalNEWS depend on agriculture and tropical forest coverage, fertilizer application, animal
338 grazing, sewage input, atmospheric N deposition and biological N fixation (Mayorga et al., 2010). The
339 inputs of dissolved silica (DSi) are controlled by soil bulk density, precipitation, slope, and presence
340 of volcanic lithology (Beusen et al., 2009).

341 The DIN speciation is not provided by the GlobalNEWS2 model. The NH_4 and NO_3 concentrations are
342 therefore determined independently on the basis of an empirical relationship between ammonium
343 fraction (NH_4/DIN ratio) and DIN loads (Meybeck, 1982). Dissolved Oxygen (DO) concentrations are
344 extracted from the water quality criteria recommendations published by the United States
345 Environmental Protection Agency (EPA, 2009). The same source is used for phytoplankton
346 concentrations, using a chlorophyll-a to phytoplankton carbon ratio of $50 \text{ gC (gChla)}^{-1}$ (Riemann et
347 al., 1989) to convert the EPA values to carbon units used in the present study.

348 Inputs of dissolved inorganic carbon (DIC) and total Alkalinity (ALK) are calculated from values
349 reported in the GLORICH database (Hartmann et al., 2009). For each watershed, seasonal mean
350 values of DIC and ALK concentrations are estimated from measurements performed at the sampling
351 locations that are closest to the river-estuary boundary. The spatial distribution of annual inputs of
352 $\text{TOC}=\text{DOC}+\text{POC}$, DIC, and $\text{TC}=\text{TOC}+\text{DIC}$ from continental watersheds to estuaries are reported in Fig.
353 5a, 5c and 5d, respectively. The contribution of tidal wetlands to the TOC inputs is also shown (Fig.
354 5b). Overall, the TC input over the entire model domain is estimated at 4.6 Tg C yr^{-1} , which falls in
355 the lower end of previous reported estimations (Najjar et al. 2012).

356

357 **2.4.3 Inputs from tidal wetlands**

358 The DOC input of estuarine wetlands (Fig. 5b) scales to their fraction, W , of the total estuarine and is
359 calculated using the GlobalNEWS parameterization:

$$Y_{DOC} = \frac{[(E_{C_{wet}} * W) + E_{C_{dry}} * (1 - W)] * R^a * Q_{act}}{Q_{nat}} \quad (12)$$

360

$$\frac{Y_{DOC_{wet}}}{Y_{DOC}} = \frac{E_{C_{wet}} * W}{E_{C_{wet}} * W + E_{C_{dry}} * (1 - W)} \quad (13)$$

361

362 where Y_{DOC} is the DOC yield ($\text{kg C km}^{-2} \text{y}^{-1}$) calculated for the entire watershed, $Y_{DOC_{wet}}$ is the
363 estimated DOC yield from wetland areas ($\text{kg C km}^{-2} \text{y}^{-1}$), Q_{act}/Q_{nat} is the ratio between the measured
364 discharge after dam construction and before dam construction, $E_{C_{wet}}$ and $E_{C_{dry}}$ ($\text{kg C km}^{-2} \text{y}^{-1}$) are
365 the export coefficients of DOC from wetland and non-wetland soils, respectively. W is the
366 percentage of the land area within a watershed that is covered by wetlands, R is the runoff (m y^{-1})
367 and a is a unit-less calibration coefficient defining how non-point source DOC export responds to
368 runoff. The value of a is set to 0.95, consistent with the original GlobalNEWS -DOC model of Harrison
369 et al. (2005). The carbon load $Y_{DOC_{wet}}$ is then exported as a diffuse source along the relevant
370 portions of estuary. The estuarine segments receiving carbon inputs from tidal wetlands are
371 identified using the National Wetlands Inventory of the U.S. Fish and Wildlife Service (U.S. Fish and
372 Wildlife Service, 2014). The inputs from those systems are then allocated to the appropriate grid cell
373 of the model domain using GIS. The flux calculated is an annual average that is subsequently
374 partitioned between the four seasons as a function of the mean seasonal temperature, assumed to
375 be the main control of the wetland-estuarine exchange. This procedure reflects the observation that

376 in spring and early summer, DOC export is small as a result of its accumulation in the salt marshes
377 induced by the high productivity (Dai and Wiegert, 1996), (Jiang et al., 2008). In late summer and fall,
378 the higher water temperature and greater availability of labile DOC contribute to higher bacterial
379 remineralization rates in the intertidal marshes (Cai et al., 1999; Middelburg et al., 1996; Wang and
380 Cai, 2004), which induce an important export. This marsh production-recycle-export pattern is
381 consistent with the observed excess DIC signal in the offshore water (Jiang et al. 2013). DIC export
382 from tidal wetlands is neglected here because it is assumed that OC is not degraded before reaching
383 the estuarine realm. Although this assumption may lead to an overestimation of OC export from
384 marshes and respiration in estuarine water, it will not significantly affect the water $p\text{CO}_2$ and
385 degassing in the estuarine waters because mixing is faster than respiration.

386 **2.4.4 Concentrations at the estuarine mouth**

387 For each estuary, the downstream boundary is located 20 km beyond the mouth to minimize the
388 bias introduced by the choice of a fixed concentration boundary condition to characterize the ocean
389 water masses (e.g. Regnier et al., 1998). This approach also reduces the influence of marine
390 boundary conditions on the simulated estuarine dynamics, especially for all organic carbon species
391 whose concentrations are fixed at zero at the marine boundary. This assumption ignores the
392 intrusion of marine organic carbon into the estuary during the tidal cycle but allows focusing on the
393 fate of terrigenous material and its transit through the estuarine filter. DIC concentrations are
394 extracted from the GLODAP dataset (Key et al., 2004), from which ALK and pH are calculated
395 assuming CO_2 equilibrium between coastal waters and the atmosphere. The equilibrium value is
396 computed using temperature (WOA2009, Locarnini et al., 2010) and salinity (WOA2009, Antonov et
397 al. (2010)) data which vary both spatially and temporally. The equilibrium approach is a reasonable
398 assumption because differences in partial pressure $\Delta p\text{CO}_2$ between coastal waters and the
399 atmosphere are generally much smaller (0-250 μatm (Signorini et al., 2013)) than those reported for
400 estuaries ($\Delta p\text{CO}_2$ in the range 0-10000 μatm (Borges and Abril, 2012)). Salinity, DO, NO_3 , DIP and DSi

401 concentrations are derived from the World Ocean Atlas (Antonov et al., 2010; Garcia et al., 2010a;
402 Garcia et al., 2010b). NH_4 concentrations are set to zero in marine waters. For all variables, seasonal
403 means are calculated for each grid cell of the boundary.

404

405 **2.5 Biogeochemical indicators**

406 The model outputs (longitudinal profiles of concentration and reaction rates) are integrated in time
407 over the entire volume or surface of each estuary to produce the following indicators of the
408 estuarine biogeochemical functioning (Regnier et al., 2013b): the mean annual Net Ecosystem
409 Metabolism (NEM), the air-water CO_2 flux (FCO_2), the carbon and nitrogen filtering capacity ($CFilt$
410 and $NFilt$) and their corresponding element budgets. The NEM (molC y^{-1}) (Caffrey, 2004; Odum,
411 1956) is defined as the difference between net primary production (NPP) and total heterotrophic
412 respiration (HR) at the system scale:

$$NEM = \int_0^{365} \int_0^L [NPP(x, t) - R_{aer}(x, t) - R_{den}(x, t)] * B(x) * H(x, t) dx dt \quad (14)$$

413

414 where NPP is the Net Primary Production ($\text{mol C m}^{-3} \text{y}^{-1}$), R_{aer} the aerobic degradation of organic
415 matter (in $\text{mol C m}^{-3} \text{y}^{-1}$) and R_{den} the denitrification (in $\text{mol C m}^{-3} \text{y}^{-1}$) (see Volta et al., 2014 for
416 detailed formulations). NEM is thus controlled by the production and decomposition of
417 autochthonous organic matter, by the amount and degradability of organic carbon delivered by
418 rivers and tidal wetlands and by the export of terrestrial and in-situ produced organic matter to the
419 adjacent coastal zone. Following the definition of NEM , the trophic status of estuaries can be net
420 heterotrophic ($NEM < 0$) when HR exceeds NPP or net autotrophic ($NEM > 0$), when NPP is larger than
421 HR because the burial and export of autochthonous organic matter exceeds the decomposition of
422 river-borne material.

423 The FCO_2 (mol C y^{-1}) is defined as:

$$FCO_2 = \int_0^{365} \int_0^L RCO_2(x, t) * B(x) dx dt \quad (15)$$

424

$$RCO_2(x, t) = -v_p(x, t) ([CO_2(aq)](x, t) - K_0(x, t) * P_{CO_2}(x, t)) \quad (16)$$

425

426 where RCO_2 (molC $m^{-2} y^{-1}$) is the rate of exchange in CO_2 at the air-water interface per unit surface
427 area, v_p is the piston velocity ($m y^{-1}$) and is calculated according to Regnier et al. (2002) to account
428 for the effect of current velocity and wind speed, $[CO_2(aq)]$ is the concentration of CO_2 in the
429 estuary ($mol m^{-3}$), K_0 is Henry's constant of CO_2 in sea water ($mol m^{-3} atm^{-1}$) and P_{CO_2} is the
430 atmospheric partial pressure in CO_2 (atm).

431 The carbon filtering capacity (in %) corresponds to the fraction of the river-borne supply that is lost
432 to the atmosphere and is defined here as the ratio of the net outgassing flux of CO_2 and the total
433 inputs of C, e.g. total carbon expressed as the sum of inorganic and organic carbon species, both in
434 the dissolved and particulate phases.

$$CFilt = \frac{FCO_2}{\int_0^{365} Q * [TC]_{riv} dt} * 100 \quad (17)$$

436 where $[TC]_{riv}$ denote the total concentrations of C in the riverine inputs.

437 Fluxes per unit area for FCO_2 and NEM , noted $\overline{FCO_2}$ and \overline{NEM} , respectively, are defined in $mol C m^{-2}$
438 y^{-1} and are calculated by dividing the integrated values calculated above by the (idealized) estuarine
439 surface S :

$$\overline{NEM} = \frac{NEM}{S} * 1000 \quad (18)$$

$$\overline{FCO_2} = \frac{FCO_2}{S} * 1000 \quad (19)$$

442 Seasonal values for the biogeochemical indicators are calculated using the same formula as above,
443 but calculate the integral over a seasonal rather than annual timescale (i.e. 3 months).

444

445

446 **2.6 Model-data comparison**

447 C-GEM has been specifically designed for an application on a global/regional scale requiring the
448 representation of a large number of individual and often data-poor systems. Maximum model
449 transferability and minimum validation requirements were thus central to the model design process
450 and the ability of the underlying approach in reproducing observed dynamics with minimal
451 calibration effort has been extensively tested. The performance C-GEM's one-dimensional
452 hydrodynamic and transport models using idealized geometries have been evaluated for a number
453 of estuarine systems exhibiting a wide variety of shapes (Savenije, 2012). In particular, it has been
454 shown that the estuarine salt intrusion can be successfully reproduced using the proposed modeling
455 approach (Savenije 2005; Volta et al., 2014; 2016b). In addition, C-GEM's biogeochemistry has also
456 been carefully validated for geometrically contrasting estuarine system in temperate climate zones.
457 Simulations for the Scheldt Estuary (Belgium and the Netherlands), a typical funnel-shaped estuary,
458 were validated through model-data and model-model comparison (Volta et al., 2014; Volta et al.,
459 2016a). Furthermore, simulations for the Elbe estuary (Germany), a typical prismatic shape estuary
460 that drains carbonate terrains and, thus, exhibits very high pH was validated against field data (Volta
461 et al., 2016a). In addition, C-GEM carbon budgets have been compared budget derived from
462 observations for 6 European estuaries discharging in the North Sea (Volta et al., 2016a). Although C-
463 GEM has been specifically designed and tested for the type of regional application presented here,
464 its transferability from North Sea to US East Coast estuaries was further evaluated by assessing its
465 performance in two East Coast estuaries. First, the hydrodynamic and transport model was tested

466 for the Delaware Bay (MAR). The model was forced with the monthly, minimal and maximal
467 observed discharge at Trenton over the period between 1912 and 1985 (UNH/GRDC Database,
468 Fekete et al., 2000). Simulated salinity profiles are compared with salinity observations from January,
469 February, May and June (the months with the highest number of data entries), which were extracted
470 from the UNH/GRDC Database. Figure 6 shows that the model captures both the salinity intrusion
471 length and the overall shape of the salinity profile well. In addition, the performance of the
472 biogeochemical model and specifically its ability to reproduce pH and pCO₂ profiles was evaluated by
473 a model-data comparison for both the Delaware Bay (MAR) in July 2003 and the Altamaha river
474 estuary (SAR) in October 1995. Similar to Volta et al., 2016a, the test systems were chosen due to
475 their contrasting geometries. The Delaware Bay is a marine dominated system characterized by a
476 pronounced funnel shape, while the Altamaha River has a prismatic estuary characteristic of river
477 dominated systems (Jiang et al., 2008). Monthly upstream boundary conditions for nutrients, as well
478 as observed pH data and calculated pCO₂ are extracted from datasets described in (Sharp, 2010) and
479 (Sharp et al., 2009) for the Delaware and in (Cai and Wang, 1998; Jiang et al., 2008) and (Cai et al.,
480 1998) for the Altamaha river estuary. The additional forcings and boundary conditions are set
481 similarly to the simulation for 2000 (see Tab. 2, 3, 4, 5, 6 in SI). Figure 7 shows that measured and
482 simulated pH values are in good agreement with observed pH and observation-derived calculations
483 of pCO₂. In the Delaware Bay, a pH minimum is located around km 140 and is mainly caused by
484 intense nitrification sustained by large inputs of NH₄ from the Philadelphia urban area, coupled to an
485 intense heterotrophic activity. Both processes lead to a well-developed pCO₂ increase in this area
486 (Fig. 7b). Although no pCO₂ data were available for validation for the period from which boundary
487 conditions were extracted, the simulated profile agree with pCO₂ measurement from July 2013
488 presented by Joesoef et al. (2015) with pCO₂ values close to equilibrium with the atmosphere in the
489 widest section of the Delaware Bay (close to the estuarine mouth) and values above 1200 μatm at
490 salinities below 5. For the Altamaha river estuary, pH steadily increases from typical river to typical
491 coastal ocean values (Fig. 7b). In addition, both observations and model results reveal that

492 outgassing is very intense in the low-salinity region with more than a 5 fold decrease in $p\text{CO}_2$
493 between salinity 0 and 5 (Fig. 7d).

494 While such local validations allow assessing the performance of the model for a specific set of
495 conditions, the purpose of this study is to capture the average biogeochemical behavior of the
496 estuaries of the eastern coast of the US. Therefore, in addition to the system-specific validation,
497 published annually averaged FCO_2 estimates for 13 tidal systems located within the study area
498 collected over the 1994-2006 period are compared to simulated FCO_2 for conditions representative
499 of the year 2000. Overall, simulated FCO_2 are comparable to values reported in the literature (Tab.
500 2). Although discrepancies, which sometimes can significant, are observed at the level of individual
501 systems, the model captures remarkably well the overall trend in CO_2 evasion rate across estuaries.
502 The model simulates low CO_2 efflux ($< 5 \text{ mol C m}^{-2} \text{ yr}^{-1}$) for the 7 systems where such conditions have
503 been observed, while the 6 systems for which the CO_2 evasion exceeds $10 \text{ mol C m}^{-2} \text{ yr}^{-1}$ are the same
504 in the observations and in the model runs. The discrepancy at the individual system level likely result
505 from a combination of factors, including the choice of model processes and their parametrization,
506 the uncertainties in constraining boundary conditions and the limited representability of
507 instantaneous and local observed.

508 **3 Results and discussion**

509 **3.1 Spatial variability of estuarine carbon dynamics**

510 Figure 8 presents the spatial distribution of simulated mean annual $\overline{\text{FCO}_2}$ and $-\overline{\text{NEM}}$ (Fig. 8a), as well
511 as FCO_2 and $-\text{NEM}$ (Fig. 8b). In general, mean annual $\overline{\text{FCO}_2}$ are about 30% larger than mean annual
512 $\overline{\text{NEM}}$, with the exception of six estuaries situated in the North of the coastal segment. Overall, the
513 $\overline{\text{NEM}}$ is characterized by smaller system to system variability compared to the $\overline{\text{FCO}_2}$ in all regions. In
514 addition, Fig. 8 reveals distinct differences across the three coastal segments and highlights the

515 important influence of the estuarine geometry and residence time, as well as the latitudinal
516 temperature gradient on estuarine carbon cycling.

517 Overall, $\overline{FCO_2}$ values are the lowest in the NAR (mean flux = $17.3 \pm 16.4 \text{ mol C m}^{-2} \text{ y}^{-1}$; surface
518 weighted average = $23.1 \text{ mol C m}^{-2} \text{ y}^{-1}$), consistent with previously reported very low values for small
519 estuaries surrounding the Gulf of Maine (Hunt et al., 2010; 2011; Tab. 2). In contrast, \overline{NEM} reveals a
520 regional minimum in the NAR ($-51.2 \pm 16.6 \text{ mol C m}^{-2} \text{ y}^{-1}$; surface weighted average = $-52.8 \text{ mol C m}^{-2}$
521 y^{-1}). The MAR is characterized by intermediate values for $\overline{FCO_2}$, with a mean flux of $26.3 \pm 34.6 \text{ mol}$
522 $\text{C m}^{-2} \text{ y}^{-1}$ (surface weighted average = $11.1 \text{ mol C m}^{-2} \text{ y}^{-1}$) and lowest values for \overline{NEM} ($-15.1 \pm 14.2 \text{ mol}$
523 $\text{C m}^{-2} \text{ y}^{-1}$; surface weighted average = $-7.4 \text{ mol C m}^{-2} \text{ y}^{-1}$). This region also shows the largest variability
524 in CO_2 outgassing compared to the NAR and SAR, with the standard deviation exceeding the mean
525 $\overline{FCO_2}$, and individual estimates ranging from $3.9 \text{ mol C m}^{-2} \text{ y}^{-1}$ to $150.8 \text{ mol C m}^{-2} \text{ y}^{-1}$. This variability
526 is mainly the result of largely variable estuarine surface areas and volumes. Some of the largest East
527 coast estuaries (e.g. Chesapeake and Delaware Bays), as well as some of smallest estuaries (e.g. York
528 River and Hudson River estuaries, Raymond et al., 1997; 2000), are located in this region (Tab. 2 and
529 4). The maximum values of $150.8 \text{ mol C m}^{-2} \text{ y}^{-1}$ simulated in the MAR are similar to the highest FCO_2
530 reported in the literature ($132.3 \text{ mol C m}^{-2} \text{ y}^{-1}$ for the Tapti estuary in India; Sarma et al., 2012). The
531 SAR is characterized by the highest mean $\overline{FCO_2}$ ($46.7 \pm 33.0 \text{ mol C m}^{-2} \text{ y}^{-1}$; surface weighted average
532 = $40.0 \text{ mol C m}^{-2} \text{ y}^{-1}$) and intermediate \overline{NEM} ($-36.8 \pm 24.7 \text{ mol C m}^{-2} \text{ y}^{-1}$; surface weighted average = -
533 $31.2 \text{ mol C m}^{-2} \text{ y}^{-1}$).

534 The NAR is characterized by a regional minimum in $\overline{FCO_2}$, and only contributes 4.6% to the total
535 FCO_2 of the East coast of the US, owing to the small cumulative surface area available for gas
536 exchange in its 10 estuarine systems. In contrast, the 18 MAR estuaries, with their large relative
537 contribution to the total regional estuarine surface area, account for as much as 70.1% of the total
538 outgassing. Because of their smaller cumulated surface area compared to those of the MAR, the 14
539 SAR estuaries account for merely 25.3% of the total outgassing despite their regional maximal $\overline{FCO_2}$.

540 A similar, yet slightly less pronounced pattern emerges for the \overline{NEM} . The NAR, MAR and SAR
541 respectively contribute 13.7%, 60.7% and 25.6% to the total regional net ecosystem metabolism. The
542 comparatively larger relative contribution of the NAR to the total NEM as compared to the total
543 FCO_2 can be explained by the importance of the specific aspect ratio for NEM . A larger ratio of
544 estuarine width b_0 and convergence length b corresponds to a more funnel shaped estuary while a
545 low ratio corresponds to a more prismatic geometry (Savenije, 2000; Volta et al., 2014). In the NAR,
546 estuaries are generally characterized by relatively narrow widths and deep-water depths, thus
547 limiting the potential surface area for gas exchange with the atmosphere. However, the relative
548 contribution of each region to the total regional NEM and FCO_2 is largely controlled by estuarine
549 surface area. Figure 9 illustrates the cumulative NEM (a) and FCO_2 (b) as a function of the cumulative
550 estuarine surface areas. The disproportionate contribution of large estuaries from the MAR
551 translates into a handful of systems (Chesapeake and Delaware Bays and the main tributaries of the
552 former, in particular) contributing to roughly half of the regional NEM and FCO_2 , in spite of relatively
553 low individual rates per unit surface area. However, the smallest systems (mostly located in the NAR
554 and SAR) nevertheless still contribute a significant fraction to the total regional NEM and FCO_2 . The
555 27 smallest systems merely account for less than 10% of the total regional estuarine surface area,
556 yet contribute 38% and 29% to the total regional NEM and FCO_2 , respectively (Fig. 9). This
557 disproportioned contribution can be mainly attributed to their high individual $\overline{FCO_2}$ and \overline{NEM} . This
558 is illustrated by the average simulated $\overline{FCO_2}$ for all 27 smallest systems (calculated as the sum of
559 each estuarine CO_2 outgassing per unit surface area divided by the total number of estuarine
560 systems) which is significantly higher ($30.2 \text{ mol C m}^{-2} \text{ y}^{-1}$) than its surface weighted average (14 mol C
561 $\text{m}^{-2} \text{ y}^{-1}$). Thereby accounting for the disproportionate contribution of very large systems (calculated
562 as the sum of each estuarine CO_2 outgassing divided by the total estuarine surface area across the
563 region).

564 Following the approach used in Regnier et al. (2013), the contribution of each biogeochemical
565 process to FCO_2 is assessed by evaluating their individual contribution to DIC and ALK changes taking
566 into account the local buffering capacity of an ionic solution when TA and DIC are changing due to
567 internal processes, but ignoring advection and mixing (Zeebe and Wolf-Gladrow 2001). In the
568 present study, we quantify the effect of the NEM on the CO_2 balance, which is almost exclusively
569 controlled by aerobic degradation rates because the contributions of denitrification and NPP to the
570 net ecosystem balance are small. Nitrification, a process triggered by the transport and/or
571 production of NH_4 in oxygenated waters, favors outgassing through its effect on pH, which shifts the
572 acid-base equilibrium of carbonate species and increases the CO_2 concentration. The contribution of
573 supersaturated riverine waters to the overall estuarine CO_2 dynamics is calculated as difference
574 between all the other processes creating or consuming CO_2 . Figure 10a presents the contribution of
575 the annually integrated *NEM*, nitrification and evasion of supersaturated, DIC enriched riverine
576 waters to the total outgassing for each system, as well as for individual regions of the domain. The
577 calculation of these annual values is based on the sum of the seasonal fluxes. Model results reveal
578 that, regionally, the *NEM* supports about 50% of the estuarine CO_2 outgassing, while nitrification and
579 riverine DIC inputs sustain about 17% and 33% of the CO_2 emissions, respectively. The relative
580 significance of the three processes described above shows important spatial variability. In the NAR,
581 oversaturated riverine waters and *NEM* respectively sustain 50% and 44% of the outgassing within
582 the sub-region, while nitrification is of minor importance (6%). In the MAR, the contribution of
583 riverine DIC inputs is significantly lower (~30%) and the main contribution to the outgassing is *NEM*
584 (~50%); nitrification accounting for slightly less than 20% of the outgassing. In the SAR, the riverine
585 contribution is even lower (~20%), and the outgassing is mainly attributed to the *NEM* (~55%) and
586 nitrification (~25%). Therefore, although the model results reveal significant variability across
587 individual systems, a clear latitudinal trend in the contribution to the total FCO_2 emerge from the
588 analysis; the importance of oversaturated riverine water decreasing from North to South, while *NEM*
589 and nitrification increase along the same latitudinal gradient. The increasing relative importance of

590 estuarine biogeochemical processes over riverine DIC inputs as drivers of FCO_2 along the North-
591 South gradient is largely driven by increasing temperatures from North to South, especially in the
592 SAR region (Tab. SI 1).

593 Contrasting patterns across the 3 regions can also be observed with respect to carbon filtering
594 capacities, $CFilt$ (Fig. 10b). In the NAR, over 90% of the riverine carbon flux is exported to the coastal
595 ocean. However, in the MAR, the high efficiency of the largest systems in processing organic carbon
596 results in a regional $CFilt$ that exceeds 50%. This contrast between the NAR and the MAR and its
597 potential implication for the carbon dynamics of the adjacent continental shelf waters has already
598 been discussed by Laruelle et al. (2015). In the NAR, short estuarine residence results in a much
599 lower removal of riverine carbon by degassing compared to the MAR. Laruelle et al. (2015)
600 suggested that this process could contribute to the weaker continental shelf carbon sink adjacent to
601 the NAR, compared to the MAR. In the SAR, most estuaries remove between 40% and 65% of the
602 carbon inputs. The high temperatures observed and resulting accelerated biogeochemical process
603 rates in this region favor the degradation of organic matter and contribute to increase the estuarine
604 filtering capacity for carbon. However, in the SAR, a large fraction of the OC loads is derived from
605 adjacent salt marshes located along the estuarine salinity gradients, thereby reducing the overall
606 residence time of OC within the systems. The filtering capacity of the riverine OC alone, which
607 transits through the entire estuary, would thus be higher than the one calculated here. As a
608 consequence, highest C retention rates are expected in warm tidal estuaries devoid of salt marshes
609 or mangroves (Cai, 2011).

610 **3.2 Seasonal variability of estuarine carbon dynamics**

611 Carbon dynamics in estuaries of the US East coast not only show a marked spatial variability, but also
612 vary on the seasonal timescale. Table 5 presents the seasonal distribution of NEM and FCO_2 for each
613 sub-region. In the NAR, a strong seasonality is simulated for the NEM and the summer period
614 contributes more than a third to the annually integrated value. The outgassing reveals a lower

615 seasonal variability and is only slightly higher than summer outgassing during fall and lower during
616 spring. In the MAR, summer contributes more to the *NEM* (>28% of the yearly total) than any other
617 season, but seasonality is less pronounced than in the NAR. Here, FCO_2 is largest in winter and
618 particularly low during summer. In the SAR, summer accounts for 30 % of the *NEM*, while spring
619 contributes 21 %. FCO_2 is relatively constant throughout the year suggesting that seasonal variations
620 in carbon processing decrease towards the lower latitudes in the SAR. This is partly related to the
621 low variability in river discharge throughout the year in lower latitudes (Tab. SI1). In riverine
622 dominated systems with low residence times, such as, for instance, the Altamaha River estuary, the
623 CO_2 exchange at the air-water interface is mainly controlled by the river discharge because the time
624 required to degrade the entire riverine organic matter flux exceeds the transit time of OC through
625 the estuary. Therefore, the riverine sustained outgassing is highest during the spring peak discharge
626 periods. In contrast, the seasonal variability in FCO_2 in long-residence, marine-dominated systems
627 with large marsh areas (e.g. Sapelo and Doboy Sound) is essentially controlled by seasonal
628 temperature variations. Its maximum is reached during summer when marsh plants are dying and
629 decomposing, as opposed to spring when marshes are in their productive stage (Jiang et al., 2008).
630 These contrasting seasonal trends have already been reported for different estuarine systems in
631 Georgia, such as the Altamaha Sound, the Sapelo Sound and the Doboy Sound (Cai, 2011). At the
632 scale of the entire East coast of the US, the seasonal trends in *NEM* reveal a clear maximum in
633 summer and minimal values during autumn and winter. The seasonality of FCO_2 is much less
634 pronounced because the outgassing of oversaturated riverine waters throughout the year
635 contributes to a large fraction of the FCO_2 and dampens the effect of the temperature dependent
636 processes (*NEM* and denitrification). In our simulations, the competition between temperature and
637 river discharge is the main driver of the seasonal estuarine carbon dynamics is. When discharge
638 increases, the carbon loads increase proportionally and the residence time within the system
639 decreases, consequently limiting an efficient degradation of organic carbon input fluxes. In warm

640 regions like the SAR, the temperature is sufficiently high all year round to sustain high C processing
641 rates and this explains the reduced seasonal variability in NEM.

642

643 **3.3 Regional carbon budget: a comparative analysis**

644 The annual carbon budget for the entire East coast of the US is summarized in Fig. 11a. The total
645 carbon input to estuaries along the East coast of the US is 4.6 Tg C yr^{-1} , of which 42% arrives in
646 organic form and 58% in inorganic form. Of this total input, saltmarshes contribute 0.6 Tg C yr^{-1} ,
647 which corresponds to about 14% of the total carbon loads and 32% of the organic loads in the
648 region. The relative contribution of the saltmarshes to the total carbon input increases towards low
649 latitudes and is as high as 60% in the SAR region. Model results suggest that 2.7 Tg C yr^{-1} is exported
650 to the continental shelf (25% as TOC and 75% as DIC), while 1.9 Tg C yr^{-1} is emitted to the
651 atmosphere. The overall carbon filtering capacity of the region thus equals 41% of the total carbon
652 entering the 43 estuarine systems (river + saltmarshes). Because of the current lack of a benthic
653 module in C-GEM, the water column carbon removal occurs entirely in the form of CO_2 outgassing
654 and does not account for the potential contribution of carbon burial in sediments. The estimated
655 estuarine carbon retention presented here is thus likely a lower bound estimate. Reported to the
656 modeled surface area of the region, the total $\overline{FCO_2}$ of 1.9 Tg C yr^{-1} translates into a mean air water
657 CO_2 flux of about $14 \text{ mol C m}^{-2} \text{ yr}^{-1}$. This value is slightly higher than the estimate of $10.8 \text{ mol C m}^{-2} \text{ yr}^{-1}$
658 calculated by Laruelle et al., (2013) on the basis of local $\overline{FCO_2}$ estimates assumed to be
659 representative of yearly averaged conditions (see section 2.1). The latter was calculated as the
660 average of 13 annual $\overline{FCO_2}$ values reported in the literature (Tab. 2), irrespective of the size of the
661 systems. This approach is useful and widely used to derive regional and global carbon budgets
662 (Borges et al., 2005; Laruelle et al., 2010; Chen et al., 2013). However, it may lead to potentially
663 significant errors (Volta et al., 2016a) due to the uncertainty introduced by the spatial interpolation

664 of local measurements to large regional surface areas, while useful and widely used to derive
665 regional and global carbon budgets.

666 Regional C budgets are sparse. To our knowledge, the only other published regional assessment of
667 the estuarine carbon and CO₂ dynamics comes from a relatively well studied region: the estuaries
668 flowing into the North Sea in Western Europe (Fig. 11b). This budget was calculated using a similar
669 approach (Volta 2016a) and thus provides an ideal opportunity for a comparative assessment of C
670 cycling in these regions. However, it is important to note that there are also important differences in
671 the applied model approaches and those differences should be taken into account when comparing
672 the derived budgets. In particular, the NW European study is based on a simulation of the 6 largest
673 systems only (Elbe, Scheldt, Thames, Ems, Humber and Weser), accounting for about 40% for the
674 riverine carbon loads of the region. It assumes that the intensity of carbon processing and evasion in
675 all other smaller estuaries discharging into the North Sea (16 % of the carbon loads) can be
676 represented by the average of the 6 largest system simulation results. In addition, the Rhine-Meuse
677 system, which alone accounts for 44% of the carbon riverine inputs of the region, was treated as a
678 passive conduit with respect to carbon due to its very short freshwater residence time (Abril et al.,
679 2002). The contribution of saltmarshes to the regional carbon budget was also ignored because their
680 total surface area is much smaller than along the US East coast (Regnier et al., 2013b). Another
681 important difference is the inclusion of seasonality in the present study while the budget calculated
682 for the North Sea is derived from yearly average conditions (Volta et al., 2016a).

683 Overall, although both regions receive similar amounts of C from rivers (4.6 Tg C y⁻¹ and 5.9 Tg C y⁻¹
684 for the East coast of the US and the North Sea, respectively), they reveal significantly different C
685 filtering capacities. While the estuaries of the East coast of the US filter 41% of the riverine TC loads,
686 those from the North Sea only remove 8% of the terrestrial-derived material. This is partly due to the
687 large amounts of carbon transiting through the 'passive' Rhine-Meuse system. The regional filtering
688 capacity is higher (15%) when this system is excluded from the analysis. However, even when

689 neglecting this system, significant differences in filtering efficiencies between both regions remain.
690 FCO_2 from the North Sea estuaries (0.5 Tg C y^{-1}) is significantly lower than the 1.9 Tg C y^{-1} computed
691 for the East coast of the US. The reason for the lower evasion rate in NW European estuaries is
692 essentially twofold. First, the total cumulative surface area available for gas exchange is significantly
693 lower along the North Sea, in spite of comparable flux densities calculated using the entire estuarine
694 surface areas of both regions ($14 \text{ mol C m}^{-2} \text{ y}^{-1}$ and $23 \text{ mol C m}^{-2} \text{ y}^{-1}$ for the East coast of the US and
695 the North Sea, respectively). Second, although the overall riverine carbon loads are comparable in
696 both regions (Fig. 11), the ratio of organic to inorganic matter input is much lower in the North Sea
697 area because of the regional lithology is dominated by carbonate rocks and mixed sediments that
698 contain carbonates (Dürr et al., 2005; Hartmann et al., 2012). As a consequence, TOC represents less
699 than 20% of the riverine loads and only 10% of the carbon exported to the North Sea. In both
700 regions, however, the increase of the inorganic to organic carbon ratio between input and output is
701 sustained by a negative NEM (Fig. 11). Although the ratios themselves may significantly vary from a
702 region of the world to the other as evidenced by these two studies, a NEM driven increase of the
703 inorganic fraction within carbon load along the estuarine axis is consistent with the global estuarine
704 carbon budget proposed by Bauer et al. (2013). In the East coast of the US, the respiration of riverine
705 OC within the estuarine filter is partly compensated by OC inputs from marshes and mangroves in
706 such a way that the input and export IC/OC ratios are closer than in the North Sea region.

707 **3.4 Scope of applicability and model limitations**

708 Complex multidimensional models are now increasingly applied to quantitatively explore carbon and
709 nutrient dynamics along the land-ocean transition zone over seasonal and even annual timescales
710 (Garnier et al., 2001; Arndt et al., 2007, 2009; Arndt and Regnier, 2007; Mateus et al., 2012).
711 However, the application of such complex models remains limited to individual, well-constrained
712 systems due their high data requirements and computational demand resulting from the need to
713 resolve important physical, biogeochemical and geological processes on relevant temporal and

714 spatial scales. The one-dimensional, computationally efficient model C-GEM has been specifically
715 designed to reduce data requirements and computational demand and to enable regional/global
716 scale applications (Volta et al., 2014, 2016a). However, such a low data demand and computational
717 efficiency inevitably requires simplification. The following paragraphs critically discuss these
718 simplifications and their implications.

719 *Spatial resolution*

720 Here, C-GEM is used with a 0.5° spatial resolution. While this resolution captures the features of
721 large systems, it is still very coarse for relatively small watershed, such as those of the St. Francis
722 River, Piscataqua River, May River or the Sapelo River. For instance, the 5 estuaries reported by Hunt
723 et al. (2010, 2011, see section 2.6) are all small systems contained by the same watershed at a 0.5°
724 resolution. Only watersheds whose area spans several grid cells can be properly identified and
725 represented (i.e. Merrimack or Penobscot with 6 and 9 cells, respectively).

726

727 *Hydrodynamic and Transport Model*

728 C-GEM is based on a theoretical framework that uses idealized geometries and significantly reduces
729 data requirements. These idealized geometries are fully described by three, easily obtainable
730 geometrical parameters (B , b_0 , H). The model thus approximates the variability of estuarine width
731 and cross-section along the longitudinal axis through a set of exponential functions. A
732 comprehensive sensitivity study (Volta et al., 2014) has shown that integrated process rates are
733 generally sensitive to changes in these geometrical parameters because of their control on estuarine
734 residence times. For instance, Volta et al. (2014) demonstrated that the NEM, is particularly sensitive
735 to the convergence length. Similarly, the use of constant depth profile may lead to variations of
736 about 10% in NEM (Volta et al., 2014). Nevertheless, geometrical parameters are generally easy to
737 constrain, especially well-monitored regions such as the US east coast. Here, all geometrical
738 parameters are constrained on the basis of observed estuarine surface areas and average water

739 depths. In addition, the model also accounts for the slope of the estuarine channel. This approach
740 ensures that simulated estuarine surface areas, volumes and, thus, residence times are in good
741 agreement with those of the real systems and minimizes uncertainties associated to the physical set-
742 up.

743 In addition, the one-dimensional representation of the idealized estuarine systems does not resolve
744 two- or three-dimensional circulation features induced by complex topography and density driven
745 circulation. While C-GEM performs well in representing the dominant longitudinal gradients, its
746 applicability to branched systems or those with aspect ratios for which a dominant axis is difficult to
747 identify (e.g. Blackwater estuary, UK; Pearl River estuary, China; Tagus estuary, Portugal; Bay of
748 Brest, France) is limited.

749 *Biogeochemical Model*

750 Although the reaction network of C-GEM accounts for all processes that control estuarine FCO_2
751 (Borges and Abril, 2012; Cai, 2011), several, potentially important processes, such as benthic-pelagic
752 exchange processes, phosphorous sorption/desorption and mineral precipitation, a more complex
753 representation of the local phytoplankton community, grazing by higher trophic levels, or multiple
754 reactive organic carbon pools are not included. Although these processes are difficult to constrain
755 and their importance for FCO_2 is uncertain, the lack of their explicit representations induces
756 uncertainties in C_{filt} . In particular, the exclusion of benthic processes such as organic matter
757 degradation and burial in estuarine sediments could result in an underestimation of C_{filt} . However,
758 because very little is known on the long term fate of organic carbon in estuarine sediments, setting
759 up and calibrating a benthic module proves a difficult task. Furthermore, to a certain degree model
760 parameters (such as organic matter degradation and denitrification rate constant) implicitly account
761 for benthic dynamics. We nonetheless acknowledge that, by ignoring benthic processes and burial in
762 particular, our estimates for the estuarine carbon filtering may be underestimated, particularly in
763 the shallow systems of the SAR.

764 Biogeochemical model parameters for regional and global applications are notoriously difficult to
765 constrain (Volta et al., 2016b). Model parameters implicitly account for processes that are not
766 explicitly resolved and their transferability between systems is thus limited. In addition, published
767 parameter values are generally biased towards temperate regions in industrialized countries (Volta
768 et al., 2016b). A first order estimation of the parameter uncertainty associated to the estuarine
769 carbon removal efficiency (C_{filt}) can be extrapolated from the extensive parameter sensitivity
770 analyses carried out by Volta et al. (2014, 2016b). These comprehensive sensitivity studies on end-
771 member systems have shown that the relative variation in C_{filt} when a number of key
772 biogeochemical parameters are varied by two orders of magnitude varies by $\pm 15\%$ in prismatic
773 (short residence time on order of days) to $\pm 25\%$ in funnel-shaped (long residence time) systems.
774 Thus, assuming that uncertainty increases linearly between those bounds as a function of residence
775 time, an uncertainty estimate can be obtained for each of our modelled estuary. With this simple
776 method, the simulated regional C_{filt} of 1.9 Tg C yr⁻¹ would be associated with an uncertainty range
777 comprised between 1.5 and 2.2 Tg C yr⁻¹. Our regional estuarine CO₂ evasion estimate is thus
778 reported with moderate confidence. Furthermore, in the future, this uncertainty range could be
779 further constrained using statistical methods such as Monte Carlo simulations (e.g. Lauerwald et al.,
780 2015).

781 *Boundary Conditions and Forcings*

782 In addition, simulations are only performed for climatological means over the period 1990-2010
783 without resolving interannual and secular variability. Boundary conditions and forcings are critical as
784 they place the modelled system in its environmental context and drive transient dynamics. However,
785 for regional applications, temporally resolved boundary conditions and forcings are difficult to
786 constrain. C-GEM places the lower boundary condition 20 km from the estuarine mouth into the
787 coastal ocean and the influence of this boundary condition on simulated biogeochemical dynamics is
788 thus limited. At the lower boundary condition, direct observations for nutrients and oxygen are

789 extracted from databases such as the World Ocean Atlas (Antonov et al., 2014). However, lower
790 boundary conditions for OC and pCO₂ (zero concentration for OC and assumption of pCO₂
791 equilibrium at the sea side) are simplified. This approach does not allow addressing the additional
792 complexity introduced by biogeochemical dynamics in the estuarine plume (see Arndt et al., 2011).
793 Yet, these dynamics only play a secondary role in the presented study that focuses on the role of the
794 estuarine transition zone in processing terrestrial-derived carbon.

795 Constraining upper boundary conditions and forcings is thus more critical. Here, C-GEM is forced by
796 seasonally-averaged conditions for Q, T, and radiation. To date, GlobalNEWS only provide yearly-
797 averaged conditions for a number of upper boundary conditions (Seitzinger et al., 2005; Mayorga et
798 al., 2010), representative of the year 2000. Simulations are thus only partly transient (induced by
799 seasonality in Q, T and radiation) and do not resolve short-lived events such as storms or extreme
800 drought conditions. In addition, direct observations of upper boundary conditions are rarely
801 available- in particular over seasonal or annual timescales. For the US East Coast estuaries, direct
802 observations are only available for O₂, chlorophyll a, DIC and Alk. For DIC and alkalinity and boundary
803 conditions are constrained by calculating the average concentration over a period of about three
804 decades. In addition, observational data is extracted at the station closest to the model's upper
805 boundary, which might be still located several kilometres upstream or downstream of the model
806 boundary. Upper boundary conditions of POC, DOC, DIN, DIP, DSi are extracted from GlobalNews
807 and thus model-derived. As a consequence, our results are thus intimately dependent on the
808 robustness of the GlobalNEWS predictions. These values are usually only considered robust
809 estimates for watersheds larger than ~10 cells (Beusen et al., 2005), which only correspond to 13 of
810 the 43 estuaries modelled in this study.

811 *Model-data comparison*

812 The generic nature of the applied model approach and, in particular the application of
813 seasonally/annually averaged or model-deduced boundary conditions renders a direct validation of

814 model results on the basis of local and instantaneous observational data (e.g. longitudinal profiles),
815 which is likely not representative of these long-term average conditions, difficult. Therefore, model
816 performance is evaluated on the basis of spatially aggregated estimates (e.g. regional FCO_2 estimates
817 based on local measurements) rather than system-to-system comparisons with longitudinal profile
818 from specific days. However, note that the performance of C-GEM has been intensively tested by
819 specific model-data comparisons for a number of different systems (e.g. Volta et al., 2014, 2016a)
820 and we are thus confident of its predictive capabilities.

821 Despite the numerous simplifying assumptions inevitably required for such a regional assessment of
822 carbon fluxes along the land-ocean continuum, the presented approach does nevertheless provide
823 an important step forward in evaluating the role of land-ocean transition systems in the global
824 carbon cycle. It provides a first robust estimate of carbon dynamics based on a theoretically well-
825 founded and carefully tested, spatially and temporally resolved model approach. This approach
826 provides novel insights that go beyond those gained through traditionally applied zero-salinity
827 method or box model approaches. In addition, it also highlights critical variables and data gaps and
828 thus helps guide efficient monitoring strategies.

829 **3.5 Towards predictors of the estuarine carbon processing**

830 The mutual dependence between geometry and transport in tidal estuaries and, ultimately, their
831 biogeochemical functioning (Savenije, 1992; Volta et al., 2014) allows relating easily extractable
832 parameters linked to their shape or their hydraulic properties to biogeochemical indicators. In this
833 section, we explore the relationships between such simple physical parameters and indicators of the
834 estuarine carbon processing \overline{NEM} , $\overline{FCO_2}$ and $CFilt$. In order to account for the effect of temperature
835 on C dynamics, \overline{NEM} and $\overline{FCO_2}$ are also normalized to the same temperature (arbitrarily chosen to
836 be 0 degree). These normalized values are obtained by dividing \overline{NEM} and $\overline{FCO_2}$ by a Q_{10} function
837 $f(T)$ (see Volta et al., 2014). This procedure allows accounting for the exponential increase in the rate
838 of several temperature dependent processes contributing to the NEM (i.e. photosynthesis, organic

839 carbon degradation...). Applying the same normalization to \overline{NEM} and $\overline{FCO_2}$ is a way of testing how
840 intimately linked NEM and FCO_2 are in estuarine systems. Indeed linear relationships relating one to
841 the other have been reported (Mayer and Eyre, 2012). The three indicators are then investigated as
842 a function of the ratio between the estuarine surface S and the seasonal river discharge Q . The
843 surface area is calculated from the estuarine width and length, as described by equation 2, in order
844 to use a parameter which is potentially applicable to other regions for which direct estimates of the
845 real estuarine surface area is not available. Since the fresh water residence time of a system is
846 obtained by dividing volume by river discharge, the S/Q ratio is also intimately linked to residence
847 time. Here, we choose to exclude the estuarine depth from the analysis because this variable cannot
848 be easily quantified from maps or remote sensing images and would thus compromise the
849 applicability of a predictive relationship on the global scale. However, from dimensional analysis, S/Q
850 can be viewed as a water residence time normalized to meter depth of water. As shown by equation
851 3, S only requires constraining BO and width convergence length b , two parameters that can readily
852 be extracted from the Google Earth engine. Global database of river discharges, as for instance
853 RivDIS (Vörösmarty et al., 1996) are also available in such a way that the S/Q ratio can potentially be
854 extracted for all estuaries around the globe.

855 Figure 12a reveals that small values of S/Q are associated with the most negative $\overline{NEM} / f(T)$. The
856 magnitude of the \overline{NEM} then exponentially decreases with increasing values of S/Q . Estuaries
857 characterized by small values of S/Q are mainly located in the NAR sub-region and correspond to
858 small surface area, and thus short residence time systems. It is possible to quantitatively relate -
859 $\overline{NEM} / f(T)$ and S/Q through a power law function ($y = 25.85 x^{-0.64}$ with a $r^2 = 0.82$). The coefficient
860 of determination remains the same when excluding estuaries from the NAR region and the equation
861 itself is not significantly different, although those estuaries on their own do not display any
862 statistically significant trend (Tab. 6). The decrease in the intensity of the net ecosystem metabolism
863 in larger estuaries (Fig 8), characterized by high S/Q ratios, can be related to the extensive

864 consumption of the organic matter pool during its transit through the estuarine filter. However,
865 when reported to the entire surface area of the estuary, larger systems (with high values of S/Q) still
866 reveal the most negative surface integrated NEM (Fig. 12b). It can also be noted that some estuaries
867 from the NAR region display very low values of $-NEM$. These data points correspond to fall and
868 winter simulations for which the temperature was relatively cold (<5 °C) and biogeochemical
869 processing was very low.

870 The overall response of $\overline{FCO_2}/f(T)$ to S/Q is comparable to that of $-\overline{NEM}/f(T)$ (Fig. 12c), with
871 lower values of $\overline{FCO_2}$ observed for high values of S/Q . However, for $S/Q < 3$ days m^{-1} , the $\overline{FCO_2}$
872 values are very heterogeneous and contain many, low $\overline{FCO_2}$ outliers from the NAR region. These
873 data points generally correspond to low water temperature conditions which keep pCO_2 low, even if
874 the system generates enough CO_2 internally via NEM . Thus, the well-documented correlation
875 between \overline{NEM} and $\overline{FCO_2}$ (Maher and Eyre, 2012) does not seem to hold for systems with very short
876 residence times. For systems with $S/Q > 3$ days m^{-1} , we obtain a regression $FCO_2 = -0.64 \times NEM + 5.96$
877 with a r^2 of 0.46, which compares well with the relation $FCO_2 = -0.42 \times NEM + 12$ proposed by Maher
878 and Eyre (2012) who used 24 seasonal estimates from small Australian estuaries. However, our
879 results suggest that this relationship cannot be extrapolated to small systems such as those located
880 in the NAR. Figure 12d, which reports non-normalized FCO_2 reveals a monotonous increase of FCO_2
881 with S/Q . This suggests that, unlike the NEM for which the normalization by a temperature function
882 allowed explaining most of the variability; FCO_2 is mostly controlled by the water residence time
883 within the system. Discharge is the main FCO_2 driver in riverine dominated systems, while
884 interactions with marshes are driving the outgassing in marine dominated systems surrounded by
885 marshes. Net aquatic biological production (NEM being negative or near 0) in large estuaries (with
886 large S/Q) is another important reason for low FCO_2 in such systems. For example, despite the higher
887 CO_2 degassing flux in the upper estuary of the Delaware, strong biological CO_2 uptake in the mid-bay
888 and near zero NEM in the lower bay result in a much lower FCO_2 for the entire estuary (Joesoef et al.

889 2015). In systems with $S/Q < 3 \text{ days m}^{-1}$, the short residence time prevents the excess CO_2 of
890 oversaturated water from being entirely exchanged with the atmosphere and simulations reveal that
891 the estuarine waters are still oversaturated in CO_2 at the estuarine mouth. Thus, the inorganic
892 carbon, produced by the decomposition of organic matter, is not outgassed within the estuary but
893 exported to the adjacent continental shelf waters. This result is consistent with the observation-
894 based hypothesis of Laruelle et al. (2015) for the NAR estuaries. As a consequence of the distinct
895 behavior of short residence time systems, the coefficient of determination of the best-fitted power
896 law function relating $\overline{FCO_2}$ and S/Q is only significant if NAR systems are excluded ($y = 31.64 x^{-0.58}$
897 with a $r^2 = 0.70$). This thus suggest that such relationships (as well as that proposed by Maher and
898 Eyre, 2012) cannot be applied to any system but only those for which $S/Q > 3 \text{ day m}^{-1}$.

899 Finally, Fig. 12e reports the simulated mean seasonal carbon filtering capacities as a function of the
900 depth normalized residence time. Not surprisingly, and in overall agreement with previous studies
901 on nutrient dynamics in estuaries (Nixon et al., 1996), the carbon filtering capacity increases with
902 S/Q . The best statistical relation between $CFilt$ and S/Q is obtained when including all 3 regions,
903 resulting in $r^2 = 0.70$ ($y = 40.64 \log_{10}(x) + 11.84$). Very little C removal occurs in systems with $S/Q < 1$
904 day m^{-1} . For systems characterized by longer depth-normalized residence times, $CFilt$ increases
905 regularly, and reaches 100% for $S/Q > 100 \text{ day m}^{-1}$. Such high values are only observed for very large
906 estuaries from the MAR region (Delaware and Chesapeake Bays); the majority of our systems had an
907 S/Q range between 1 and 100 day m^{-1} . The quantitative assessment of estuarine filtering capacities
908 is further complicated by the complex interplay of estuarine and coastal processes. Episodically,
909 marked spatial variability in concentration gradients near the estuarine mouth may lead to a reversal
910 of net material fluxes from coastal waters into the estuary (Regnier et al., 1998; Arndt et al. 2011).
911 Our results show that this feature is particularly significant for estuaries with a large width at the
912 mouth and short convergence length (funnel shaped or 'Bay type' systems). These coastal nutrient
913 and carbon inputs influence the internal estuarine C dynamics and lead to filtering capacities that

914 can exceed 100%. This feature is particularly significant in summer, when riverine inputs are low and
915 the marine material is intensively processed inside the estuary.

916 Previous work investigated the relationship between fresh water residence time and nutrient
917 retention (Nixon et al., 1996; Arndt et al., 2011; Laruelle, 2009). These studies, however, were
918 constrained by the scarcity of data. For instance, the pioneering work of Nixon et al. (1996) only
919 relied on a very limited number (<10) of quite heterogeneous coastal systems, all located along the
920 North Atlantic. Here, our modeling approach allows us to generate 172 (43 x 4) data points, each
921 representing a system-scale biogeochemical behavior. Together, this database spans the entire
922 spectrum of estuarine settings and climatic conditions found along the East coast of the US. In
923 addition, the ratio S/Q used as master variable for predicting temperature normalized $\overline{-NEM}$, $\overline{FCO_2}$
924 and $CFilt$ only requires a few easily accessible geometric parameters ($B0$, b and L) and an estimate of
925 the river discharge. While it is difficult to accurately predict $\overline{FCO_2}$ for small systems such as those
926 located in the NAR region, the relationships found are quite robust for systems in which $S/Q > 3$ days
927 m^{-1} . Most interestingly, $CFilt$ values reveal a significant correlation with S/Q and could be used in
928 combination with global riverine carbon delivery estimates such as GlobalNews 2 (Mayorga et al.,
929 2010) to constrain the estuarine CO_2 evasion and the carbon export to the coastal ocean at the
930 continental and global scales.

931 **4. Conclusions**

932 This study presents the first complete estuarine carbon budget for the East coast of the US using a
933 modeling approach. The structure of the model C-GEM relies on a restricted number of readily
934 available global datasets to constrain boundary conditions and limits the number of geometrical and
935 physical parameters to be constrained. Our simulations predict a total CO_2 outgassing of $1.9 \text{ Tg C } y^{-1}$
936 for all tidal estuaries of the East coast of the US. This quantification accounts for the seasonality in
937 estuarine carbon processing as well as for distinct individual behaviors among estuarine types
938 (marine or river dominated). The total carbon output to the coastal ocean is estimated at $2.7 \text{ TgC } y^{-1}$,

939 and the carbon filtering capacity with respect to riverine, marshes and mangrove inputs is thus on
940 the order of 40%. This value is significantly higher than the recently estimated C filtering capacity for
941 estuaries surrounding the North Sea using a similar approach (Volta et al., 2016a), mainly because
942 the surface area available for gas exchange and the draining lithology limits the CO₂ evasion in the
943 NW European systems. At the regional scale of the US East coast estuaries, net heterotrophy is the
944 main driver (50%) of the CO₂ outgassing, followed by the ventilation of riverine supersaturated
945 waters entering the estuarine systems (32%) and nitrification (18%). The dominant mechanisms for
946 the gas exchange and the resulting carbon filtering capacities nevertheless reveal a clear latitudinal
947 pattern, which reflects the shapes of estuarine systems, climatic conditions and dominant land-use
948 characteristics.

949 Our model results are used to derive predictive relationships relating the intensity of the area-based
950 Net Ecosystem Metabolism (\overline{NEM}), air-water CO₂ exchange ($\overline{FCO_2}$) and the carbon filtering capacity
951 ($CFilt$) to the depth normalized residence time, expressed as the ratio of the estuarine surface area
952 to the river discharge. In the future, such simple relationships relying on readily available geometric
953 and hydraulic parameters could be used to quantify carbon processing in areas of the world devoid
954 of direct measurements. However, it is important to note that such simple relationships are only
955 valid over the range of boundary conditions and forcings explored and may not be applicable to
956 conditions that fall outside of this range. In regions with better data coverage, such as the one
957 investigated here, our study highlights that the regional-scale quantification, attribution, and
958 projection of estuarine biogeochemical cycling are now at reach.

959 **5. Acknowledgements**

960 G. G. Laruelle is Chargé de recherches du F.R.S.-FNRS at the Université Libre de Bruxelles. The
961 research leading to these results has received funding from the European Union's Horizon 2020
962 research and innovation programme under the Marie Skłodowska-Curie grant agreement No 643052

963 (C-CASCADES project). The authors thank V. L. Mulder for her thorough reading of the manuscript
964 upon submission.

965

966 **References:**

- 967 Abril, G., Nogueira, M., Etcheber, H., Cabeçadas, G., Lemaire, E., and Brogueira, M.J.: Behaviour of
968 organic carbon in nine contrasting European estuaries. *Estuar. Coast. Shelf Sci.*, 54, 241-262,
969 2002.
- 970 Antonov, J.I., Seidov, D., Boyer, T.P., Locarnini, R.A., Mishonov, A.V., Garcia, H.E., Baranova, O.K.,
971 Zweng, M.M., and Johnson, D.R.: *World Ocean Atlas 2009, Volume 2: Salinity*. S., 2010.
- 972 Arndt, S., Vanderborght, J.P., and Regnier, P.: Diatom growth response to physical forcing in a
973 macrotidal estuary: Coupling hydrodynamics, sediment transport, and biogeochemistry.
974 *Journal of Geophysical Research C: Oceans*, 112(5), 2007.
- 975 Arndt, S. and Regnier, P.: A model for the benthic-pelagic coupling of silica in estuarine ecosystems:
976 sensitivity analysis and system scale simulation, *Biogeosciences*, 4, 331–352, doi:10.5194/bg-
977 4-331-2007, 2007.
- 978 Arndt, S., Regnier, P., and Vanderborght, J.P.: Seasonally-resolved nutrient export fluxes and filtering
979 capacities in a macrotidal estuary. *Journal of Marine Systems*, 78(1), 42-58, 2009.
- 980 Arndt, S., Lacroix, G., Gypens, N., Regnier, P., and Lancelot, C.: Nutrient dynamics and phytoplankton
981 development along an estuary-coastal zone continuum: A model study. *Journal of Marine*
982 *Systems*, 84(3-4), 49-66, 2011.
- 983 Atlas, R., Hoffman, R.N., Ardizzone, J., Leidner, S.M., Jusem, J.C., Smith, D.K. and Gombos, D.: A
984 cross-calibrated, multiplatform ocean surface wind velocity product for meteorological and
985 oceanographic applications. *Bulletin of the American Meteorological Society*, 92(2), 157-174,
986 2011.
- 987 Baklouti, M., Chevalier, C., Bouvy, M., Corbin, D., Pagano, M., Troussellier, M., and Arfi, R.: A study of
988 plankton dynamics under osmotic stress in the Senegal River Estuary, West Africa, using a 3D
989 mechanistic model, *Ecol. Model.*, 222, 2704–2721, 2011.
- 990 Bauer, J.E., Cai, W.J., Raymond, P.A., Bianchi, T.S., Hopkinson, C.S., and Regnier, P.A.G.: The changing
991 carbon cycle of the coastal ocean. *Nature*, 504(7478), 61-70, 2013.
- 992 Beusen, A. H.W., Dekkers, A. L. M., Bouwman, A. F., Ludwig, W., and Harrison, J.: Estimation of global
993 river transport of sediments and associated particulate C, N, and P, *Global Biogeochem. Cy.*,
994 19, GB4S05, doi:10.1029/2005GB002453, 2005.
- 995 Beusen, A.H.W., Bouwman, A.F., Dürr, H.H., Dekkers, A.L.M., and Hartmann, J.: Global patterns of
996 dissolved silica export to the coastal zone: Results from a spatially explicit global model.
997 *Global Biogeochemical Cycles*, 23, GB0A02, doi:10.1029/2008GB003281, 2009.
- 998 Billen, G., Thieu, V., Garnier, J., and Silvestre, M.: Modelling the N cascade in regional waters: The
999 case study of the Seine, Somme and Scheldt rivers, *Agr. Ecosyst. Environ.*, 133, 234–246,
1000 2009.
- 1001 Borges, A.V., Delille, B., and Frankignoulle, M.: Budgeting sinks and sources of CO₂ in the coastal
1002 ocean: Diversity of ecosystems counts. *Geophys. Res. Lett.*, 32(14), L14601, 2005.
- 1003 Borges, A.V., and Abril, G.: Carbon Dioxide and Methane Dynamics in Estuaries. In: E. Wolanski and
1004 D.S. McLusky (Editors), *Treatise on Estuarine and Coastal Science*. Academic Press, Waltham,
1005 pp. 119–161, 2012.
- 1006 Bricker, S., Longstaff, B., Dennison, W., Jones, A., Boicourt, K., Wicks, C., and Woerner, J.: *Effects of*
1007 *Nutrient Enrichment In the Nation's Estuaries: A Decade of Change*, NOAA, MD, 2007.
- 1008 Brock, T.D.: Calculating solar radiation for ecological studies. *Ecological Modelling*, 14(1-2), 1-19,
1009 1981.
- 1010 Caffrey, J.: Factors controlling net ecosystem metabolism in U.S. estuaries. *Estuaries*, 27(1), 90-101,
1011 2004.
- 1012 Cai, W.J., and Wang, Y.: The chemistry, fluxes, and sources of carbon dioxide in the estuarine waters
1013 of the Satilla and Altamaha Rivers, Georgia. *Limnology and Oceanography*, 43(4), 657-668,
1014 1998.
- 1015 Cai, W.J., Wang, Y., and Hodson, R. E.: Acid-base properties of dissolved organic matter in the
1016 estuarine waters of Georgia, USA. *Geochimica et Cosmochimica Acta*, 62(3), 473-483, 1998.

- 1017 Cai, W.J., Pomeroy, L.R., Moran, M.A., and Wang, Y.: Oxygen and carbon dioxide mass balance for
 1018 the estuarine-intertidal marsh complex of five rivers in the southeastern U.S. *Limnology and*
 1019 *Oceanography*, 44, 639-649, 1999.
- 1020 Cai, W.J.: Estuarine and coastal ocean carbon paradox: CO₂ sinks or sites of terrestrial carbon
 1021 incineration? *Ann. Rev. Mar. Sci.*, 3, 123-145, 2011.
- 1022 Cerco, C., Kim, S.-C., and Noel, M.: The 2010 Chesapeake Bay eutrophication model. US
 1023 Environmental Protection Agency Chesapeake Bay Program, Annapolis, MD, 2010.
- 1024 Chen, C.-T.A., Huang, T.-H., Fu, Y.-H., Bai, Y., and He, X.: Strong sources of CO₂ in upper estuaries
 1025 become sinks of CO₂ in large river plumes. *Current Opinion in Environmental Sustainability*,
 1026 4(2), 179-185, 2012.
- 1027 Chen, C.-T. A., Huang, T.-H., Chen, Y.-C., Bai, Y., He, X., and Kang, Y.: Air-sea exchanges of CO₂ in the
 1028 world's coastal seas, *Biogeosciences*, 10, 6509–6544, doi:10.5194/bg-10-6509-2013, 2013.
- 1029 Dai, T., and Wiegert, R.G.: Estimation of the primary productivity of *Spartina alterniflora* using a
 1030 canopy model. *Ecography*, 19(4), 410-423, 1996.
- 1031 Dufore, C. M.: Spatial and Temporal Variations in the Air-Sea Carbon Dioxide Fluxes of Florida Bay,
 1032 Graduate School Thesis, University of South Florida, 2012.
- 1033 Dürr, H.H., Meybeck, M., and Dürr, S.H.: Lithological composition of the Earth's continental surfaces
 1034 derived from a new digital map emphasizing riverine material transfer. *Glob. Biogeochem.*
 1035 *Cycles* 19 (4), GB4S10, 2005.
- 1036 Dürr, H.H., Laruelle, G.G., van Kempen, C.M., Slomp, C.P., Meybeck, M., and Middelkoop, H.:
 1037 Worldwide Typology of Nearshore Coastal Systems: Defining the Estuarine Filter of River
 1038 Inputs to the Oceans. *Estuaries and Coasts*, 34(3), 441-458, 2011.
- 1039 EPA (2009). "1970 - 2008 Average annual emissions, all criteria pollutants in MS Excel." National
 1040 Emissions Inventory (NEI) Air Pollutant Emissions Trends Data. Office of Air Quality Planning
 1041 and Standards. Available online at <<http://www.epa.gov/ttn/chief/trends/index.html>>
- 1042 Fekete, B.M., Vörösmarty, C.J., and Grabs, W.: High-resolution fields of global runoff combining
 1043 observed river discharge and simulated water balances. *Global Biogeochemical Cycles*, 16(3),
 1044 15-1, 2002.
- 1045 Fischer, H. B.: Mixing and Dispersion in Estuaries, *Annu. Rev. Fluid Mech.*, 8, 107–133,
 1046 1976. Friedrichs, M.A.M., and Hofmann, E.E.: Physical control of biological processes in the
 1047 central equatorial Pacific Ocean. *Deep-Sea Research Part I: Oceanographic Research Papers*,
 1048 48(4), 1023-1069, 2001.
- 1049 Garcia, H.E., Locarnini, R.A., Boyer, E.W., Antonov, A., Baranova, O.K., Zweng, M.M., and Johnson,
 1050 D.R.: *World Ocean Atlas 2009, Volume 3: Dissolved Oxygen, Apparent Oxygen Utilization,*
 1051 *and Oxygen Saturation*, 2010a.
- 1052 Garcia, H.E., Locarnini, R.A., Boyer, E.W., Antonov, J.I., Baranova, O.K., Zweng, M.M., and Johnson,
 1053 D.R.: *World Ocean Atlas 2009, Volume 4: Nutrients (phosphate, nitrate, silicate)*, 2010b.
- 1054 Garnier, J., Servais, P., Billen, G., Akopian, M., and Brion, N.: Lower Seine River and Estuary (France)
 1055 Carbon and Oxygen Budgets During Low Flow, *Estuaries*, 24, 964–976, 2001.
- 1056 Harrison, J.A., Caraco, N., and Seitzinger, S.P.: Global patterns and sources of dissolved organic
 1057 matter export to the coastal zone: Results from a spatially explicit, global model. *Global*
 1058 *Biogeochemical Cycles*, 19(4), GB4S03, doi:10.1029/2004GB002357, 2005.
- 1059 Hartmann, J., Jansen, N., Dürr, H.H., Kempe, S., and Köhler, P.: Global CO₂ consumption by chemical
 1060 weathering: What is the contribution of highly active weathering regions? *Global Planet.*
 1061 *Change*, 69(4), 185-194, 2009.
- 1062 Hartmann, J., Dürr, H.H., Moosdorf, N., Meybeck, M., and Kempe, S.: The geochemical composition
 1063 of the terrestrial surface (without soils) and comparison with the upper continental crust.
 1064 *Int. J. Earth Sci.* 101, 365-376, 2012.
- 1065 Herrmann, M., Najjar, R.G., Kemp, W.M., Alexander, R.B., Boyer, E.W., Cai, W.-J., Griffith, P.C.,
 1066 Kroeger, K.D., McCallister, S.L., and Smith, R.A.: Net ecosystem production and organic

1067 carbon balance of U.S. East Coast estuaries: A synthesis approach, *Global Biogeochem.*
1068 *Cycles*, 29, doi:10.1002/2013GB004736, 2015.

1069 Hofmann, A.F., Soetaert, K., and Middelburg, J.J.: Present nitrogen and carbon dynamics in the
1070 Scheldt estuary using a novel 1-D model. *Biogeosciences*, 5(4), 981-1006, 2008.

1071 Hofmann, E.E., Cahill, B., Fennel, K., Friedrichs, M.A.M., Hyde, K., Lee, C., Mannino, A., Najjar, R.G.,
1072 O'Reilly, J.E., Wilkin, J., and Xue, J.: Modeling the dynamics of continental shelf carbon. *Ann*
1073 *Rev Mar Sci*. 3, 93-122, 2011.

1074 Hunt, C. W., Salisbury, J. E., Vandemark, D., and McGillis, W.: Contrasting Carbon Dioxide Inputs and
1075 Exchange in Three Adjacent New England Estuaries. *Estuar. Coast.*, 34, 68–77,
1076 doi:10.1007/s12237-010-9299-9, 2010.

1077 Hunt, C.W., Salisbury, J.E., Vandemark, D., and McGillis, W.: Contrasting Carbon Dioxide Inputs and
1078 Exchange in Three Adjacent New England Estuaries. *Estuaries and Coasts*, 34(1), 68-77, 2011.

1079 Ippen, A.T., and Harleman, D.R.F.: One-dimensional Analysis of Salinity Intrusion in Estuaries,
1080 Technical Bulletin No. 5, Committee on Tidal Hydraulics, Corps of Engineers, US Army,
1081 Vicksburg, 1961.

1082 Jiang, L.Q., Cai, W.J., and Wang, Y.: A comparative study of carbon dioxide degassing in river- and
1083 marine-dominated estuaries. *Limnology and Oceanography*, 53(6), 2603-2615, 2008.

1084 Jiang, L.-Q., Cai, W.-J., Wang, Y., and Bauer, J. E.: Influence of terrestrial inputs on continental shelf
1085 carbon dioxide, *Biogeosciences*, 10, 839–849, doi:10.5194/bg-10-839-2013, 2013.

1086 Joesoef, A., Huang, W.-J., Gao, Y., and Cai, W.-J.: Air–water fluxes and sources of carbon dioxide in
1087 the Delaware Estuary: spatial and seasonal variability, *Biogeosciences*, 12, 6085-6101,
1088 doi:10.5194/bg-12-6085-2015, 2015.

1089 Kent, B.H.: Turbulent diffusion in a Sectionally Homogeneous Estuary, Technical Report 16,
1090 Chesapeake Bay Institute, John Hopkins, University, Baltimore, 1958.

1091 Key, R.M., Kozyr, A., Sabine, C.L., Lee, K., Wanninkhof, R., Bullister, J.L., Feely, R.A., Millero, F.J.,
1092 Mordy, C., and Peng, T.H.: A global ocean carbon climatology: Results from Global Data
1093 Analysis Project (GLODAP). *Global Biogeochemical Cycles*, 18(4), 1-23, 2004.

1094 Laruelle, G.G.: Quantifying nutrient cycling and retention in coastal waters at the global scale, Ph D
1095 dissertation, Utrecht University, 2009.

1096 Laruelle, G. G., Regnier, P., Ragueneau, O., Kempa, M., Moriceau, B., Ni Longphuir, S., Leynaert, A.,
1097 Thouzeau, G., and Chauvaud, L.: Benthic-pelagic coupling and the seasonal silica cycle in the
1098 Bay of Brest (France): new insights from a coupled physical-biological model, *Mar. Ecol.-*
1099 *Prog. Ser.*, 385, 15–32, 2009.

1100 Laruelle, G.G., Dürr, H.H., Slomp, C.P., and Borges, A.V.: Evaluation of sinks and sources of CO₂ in the
1101 global coastal ocean using a spatially-explicit typology of estuaries and continental shelves.
1102 *Geophys. Res. Lett.*, 37(15), L15607, doi:10.1029/2010GL043691, 2010.

1103 Laruelle, G.G., Dürr, H.H., Lauerwald, R., Hartmann, J., Slomp, C.P., Goossens, N., and Regnier, P.A.G.:
1104 Global multi-scale segmentation of continental and coastal waters from the watersheds to
1105 the continental margins. *Hydrol. Earth Syst. Sci.*, 17(5), 2029-2051, 2013.

1106 Laruelle, G.G., Lauerwald, R., Rotschi, J. Raymond, P.A., and Regnier, P.: Seasonal response of air-
1107 water CO₂ exchange along the land-ocean aquatic continuum of the northeast North
1108 American coast. *Biogeosci.* 12, 1447-1458, 2015.

1109 Lauerwald, R., Hartmann, J., Moosdorf, N., Kempe, S., and Raymond, P.A.: What controls the spatial
1110 patterns of the riverine carbonate system? — A case study for North America. *Chemical*
1111 *Geology*, 337–338, 114-127, 2013.

1112 Lauerwald, R., Laruelle, G. G., Hartmann, J., Ciais, P., and Regnier, P. A. G.: Spatial patterns in CO₂
1113 evasion from the global river network, *Global Biogeochem. Cy.*, 29, 534–554,
1114 doi:10.1002/2014GB004941, 2015.

1115 Leonard, B.: Third-Order Upwinding as a Rational Basis for Computational Fluid Dynamics, in:
1116 *Computational Techniques and Applications: CTAC-83*, edited by: Noye J. and Fletcher C. A.
1117 J., Elsevier, North-Holland, 1984.

- 1118 Le Quéré, C., Peters, G. P., Andres, R. J., Andrew, R. M., Boden, T. A., Ciais, P., Friedlingstein, P.,
1119 Houghton, R. A., Marland, G., Moriarty, R., Sitch, S., Tans, P., Arneeth, A., Arvanitis, A., Bakker,
1120 D. C. E., Bopp, L., Canadell, J. G., Chini, L. P., Doney, S. C., Harper, A., Harris, I., House, J. I.,
1121 Jain, A. K., Jones, S. D., Kato, E., Keeling, R. F., Klein Goldewijk, K., Körtzinger, A., Koven, C.,
1122 Lefèvre, N., Maignan, F., Omar, A., Ono, T., Park, G.-H., Pfeil, B., Poulter, B., Raupach, M. R.,
1123 Regnier, P., Rödenbeck, C., Saito, S., Schwinger, J., Segschneider, J., Stocker, B. D., Takahashi,
1124 T., Tilbrook, B., van Heuven, S., Viovy, N., Wanninkhof, R., Wiltshire, A., and Zaehle, S.:
1125 Global carbon budget 2013, *Earth Syst. Sci. Data*, 6, 235-263, doi:10.5194/essd-6-235-2014,
1126 2014.
- 1127 Le Quéré, C., Moriarty, R., Andrew, R. M., Canadell, J. G., Sitch, S., Korsbakken, J. I., Friedlingstein, P.,
1128 Peters, G. P., Andres, R. J., Boden, T. A., Houghton, R. A., House, J. I., Keeling, R. F., Tans, P.,
1129 Arneeth, A., Bakker, D. C. E., Barbero, L., Bopp, L., Chang, J., Chevallier, F., Chini, L. P., Ciais, P.,
1130 Fader, M., Feely, R. A., Gkritzalis, T., Harris, I., Hauck, J., Ilyina, T., Jain, A. K., Kato, E., Kitidis,
1131 V., Klein Goldewijk, K., Koven, C., Landschützer, P., Lauvset, S. K., Lefèvre, N., Lenton, A.,
1132 Lima, I. D., Metzl, N., Millero, F., Munro, D. R., Murata, A., Nabel, J. E. M. S., Nakaoka, S.,
1133 Nojiri, Y., O'Brien, K., Olsen, A., Ono, T., Pérez, F. F., Pfeil, B., Pierrot, D., Poulter, B., Rehder,
1134 G., Rödenbeck, C., Saito, S., Schuster, U., Schwinger, J., Séférian, R., Steinhoff, T., Stocker, B.
1135 D., Sutton, A. J., Takahashi, T., Tilbrook, B., van der Laan-Luijkx, I. T., van der Werf, G. R., van
1136 Heuven, S., Vandemark, D., Viovy, N., Wiltshire, A., Zaehle, S., and Zeng, N.: Global Carbon
1137 Budget 2015, *Earth Syst. Sci. Data*, 7, 349-396, doi:10.5194/essd-7-349-2015, 2015.
- 1138 Lin, J., Xie, L., Pietrafesa, L. J., Ramus, J. S., and Paerl, H.W.: Water Quality Gradients across
1139 Albemarle-Pamlico Estuarine System: Seasonal Variations and Model Applications, *J. Coast.
1140 Res.*, 23, 213–229, 2007.
- 1141 Locarnini, R.A., Mishonov, A.V., Antonov, J.I., Boyer, T.P., Garcia, H.E., Baranova, O.K., Zweng, M.M.,
1142 and Johnson, D.R.: *World Ocean Atlas 2009, Volume 1: Temperature*, 2010.
- 1143 Ludwig, W., Probst, J. L., and Kempe, S.: predicting the oceanic input of organic carbon by
1144 continental erosion, *Global Biogeochem. Cy.*, 10, 23–41, 1996.
- 1145 Maher, D.T., and Eyre, B.D.: Carbon budgets for three autotrophic Australian estuaries: Implications
1146 for global estimates of the coastal air-water CO₂ flux. *Global Biogeochem. Cycles*, 26(1),
1147 GB1032, 2012.
- 1148 Mateus, M., Vaz, N., and Neves, R.: A process-oriented model of pelagic biogeochemistry for marine
1149 systems. Part II: Application to a mesotidal estuary, *J. Mar. Syst.*, 94, 90–101, 2012.
- 1150 Mayorga, E., Seitzinger, S.P., Harrison, J.A., Dumont, E., Beusen, A.H.W., Bouwman, A.F., Fekete,
1151 B.M., Kroeze, C., and Van Drecht, G.: Global Nutrient Export from WaterSheds 2 (NEWS 2):
1152 Model development and implementation. *Environmental Modelling and Software*, 25(7),
1153 837-853, 2010.
- 1154 Meybeck, M.: Carbon, nitrogen, and phosphorus transport by world rivers. *Am. J. Sci.*, 282(4), 401-
1155 450, 1982.
- 1156 Meybeck, M., Dürr, H. H., and Vörosmary, C. J.: Global coastal segmentation and its river catchment
1157 contributors: A new look at land-ocean linkage, *Global Biogeochem. Cy.*, 20, GB1S90,
1158 doi:10.1029/2005GB002540, 2006.
- 1159 Middelburg, J.J., Klaver, G., Nieuwenhuize, J., Wielemaker, A., De Haas, W., Vlug, T., and Van Der
1160 Nat, J.F.W.A.: Organic matter mineralization in intertidal sediments along an estuarine
1161 gradient. *Marine Ecology Progress Series*, 132(1-3), 157-168, 1996.
- 1162 NASA/NGA: SRTM Water Body Data Product Specific Guidance, Version 2.0, 2003.
- 1163 Najjar, R.G., Friedrichs, M., and Cai, W.-J. (Editors): Report of The U.S. East Coast Carbon Cycle
1164 Synthesis Workshop, January 19-20, 2012. Ocean Carbon and Biogeochemistry Program and
1165 North American Carbon Program, 34 pp, 2012.
- 1166 Nihoul, J. C. J., and Ronday, F.: Modèles d'estuaires partiellement stratifiés, *Projet Mer*, Vol. 10,
1167 Service de la Programmation Scientifique, Bruxelles, Belgium, 71–98, 1976.

- 1168 Nixon, S.W., J.W. Ammerman, L.P. Atkinson, V.M. Berounsky, G. Billen, W.C. Boicourt, W.R. Boynton,
1169 T.M. Church, D.M. Ditoro, R. Elmgren, J.H. Garber, A.E. Giblin, R.A. Jahnke, N.J. P. Owens,
1170 M.E.Q. Pilson, and Seitzinger, S.P.: The fate of nitrogen and phosphorus at the land–sea
1171 margin of the North Atlantic Ocean. *Biogeochemistry* 3, 141–180, 1996.
- 1172 NOAA: National Estuarine Inventory Data Atlas, Volume 1: Physical and Hydrologic Characteristics,
1173 National Oceanic and Atmospheric Administration, MD, 1985.
- 1174 Odum, H.T.: Primary Production in Flowing Waters. *Limnol. Oceanogr.*, 1, 102-117, 1956.
- 1175 O’Kane, J. P.: Estuarine Water Quality Management. Pitman, London, U.K, 1980.
- 1176 Paerl, H.W., Valdes, L.M., Peierls, B.L., Adolf, J.E., and Harding Jr, L.W.: Anthropogenic and climatic
1177 influences on the eutrophication of large estuarine ecosystems. *Limnology and*
1178 *Oceanography*, 51(1 II), 448-462, 2006.
- 1179 Platt, T., Gallegos, C. L., and Harrison, W. G.: Photoinhibition of photosynthesis in natural
1180 assemblages of marine phytoplankton. *J. Mar. Res.*, 38, 687-701, 1980.
- 1181 Preddy, W. S.: The mixing and movement of water in the estuary of the Thames, *J. Mar. biol. Ass. UK*,
1182 33, 645–662, 1954.
- 1183 Press, W. H., Teukolosky, S. A., Vetterling, W. T., and Flannery, B.P.: Numerical Recipes in C: The Art
1184 of Scientific Programming, 2nd Edn., Cambridge University Press, USA, 1992.
- 1185 Pritchard, D. W.: The Equations of Mass Continuity and Salt Continuity in Estuaries, *J. Marine Res.*,
1186 15, 33–42, 1958.
- 1187 Raymond, P.A., Caraco, N.F., and Cole, J.J.: Carbon dioxide concentration and atmospheric flux in the
1188 Hudson River. *Estuaries*, 20(2), 381-390, 1997.
- 1189 Raymond, P.A., Bauer, J.E., and Cole, J.J.: Atmospheric CO₂ evasion, dissolved inorganic carbon
1190 production, and net heterotrophy in the York River estuary. *Limnology and Oceanography*,
1191 45(8), 1707-1717, 2000.
- 1192 Raymond, P.A., and Hopkinson, C.S.: Ecosystem Modulation of Dissolved Carbon Age in a Temperate
1193 Marsh-Dominated Estuary. *Ecosystems*, 6(7), 694-705, 2003.
- 1194 Raymond, P.A., Hartmann, J., Lauerwald, R., Sobek, S., McDonald, C., Hoover, M., Butman, D., Striegl,
1195 R., Mayorga, E., Humborg, C., Kortelainen, P., Dürr, H., Meybeck, M., Ciais, P., and Guth, P.:
1196 Global carbon dioxide emissions from inland waters. *Nature*, 503(7476), 355-359, 2013.
- 1197 Regnier, P., Wollast, R., and Steefel, C.I.: Long-term fluxes of reactive species in macrotidal estuaries:
1198 Estimates from a fully transient, multicomponent reaction-transport model. *Marine*
1199 *Chemistry*, 58(1-2), 127-145, 1997.
- 1200 Regnier, P., Mouchet, A., Wollast, R., and Runday, F.: A discussion of methods for estimating residual
1201 fluxes in strong tidal estuaries, *Cont. Shelf Res.*, 18, 1543–1571, 1998.
- 1202 Regnier, P., and Steefel, C.I.: A high resolution estimate of the inorganic nitrogen flux from the
1203 Scheldt estuary to the coastal North Sea during a nitrogen-limited algal bloom, spring 1995.
1204 *Geochimica et Cosmochimica Acta*, 63(9), 1359-1374, 1999.
- 1205 Regnier, P., Vanderborcht, J. P., Steefel, C. I., and O’Kane, J. P.: Modeling complex multi-component
1206 reactive-transport systems: Towards a simulation environment based on the concept of a
1207 Knowledge Base, *Appl. Math. Model.*, 26, 913–927, 2002.
- 1208 Regnier, P., Friedlingstein, P., Ciais, P., Mackenzie, F.T., Gruber, N., Janssens, I.A., Laruelle, G.G.,
1209 Lauerwald, R., Luyssaert, S., Andersson, A.J., Arndt, S., Arnosti, C., Borges, A.V., Dale, A.W.,
1210 Gallego-Sala, A., Godderis, Y., Goossens, N., Hartmann, J., Heinze, C., Ilyina, T., Joos, F.,
1211 LaRowe, D.E., Leifeld, J., Meysman, F.J.R., Munhoven, G., Raymond, P.A., Spahni, R.,
1212 Suntharalingam, P., and Thullner, M.: Anthropogenic perturbation of the carbon fluxes from
1213 land to ocean. *Nature Geosci*, 6(8), 597-607, 2013a.
- 1214 Regnier, P., Arndt, S., Goossens, N., Volta, C., Laruelle, G.G., Lauerwald, R., and Hartmann, J.:
1215 Modelling Estuarine Biogeochemical Dynamics: From the Local to the Global Scale. *Aquatic*
1216 *Geochemistry*, 19(5-6), 591-626, 2013b.
- 1217 Riemann, B., Simonsen, P., and Stensgaard, L.: The carbon and chlorophyll content of phytoplankton
1218 from various nutrient regimes. *Journal of Plankton Research*, 11 (5), 1037-1045, 1989.

- 1219 Rossow, W.B., and Schiffer, R.A.: Advances in understanding clouds from ISCCP. *Bull. Amer.*
1220 *Meteorol. Soc.*, 80, 2261-2288, doi:10.1175/1520-0477(1999)080<2261:AIUCFI>2.0.CO;2,
1221 1999.
- 1222 Sarma, V.V.S.S., Viswanadham, R., Rao, G.D., Prasad, V.R., Kumar, B.S.K., Naidu, S.A., Kumar, N.A.,
1223 Rao, D.B., Sridevi, T., Krishna, M.S., Reddy, N.P.C., Sadhuram, Y., and Murty, T.V.R.: Carbon
1224 dioxide emissions from Indian monsoonal estuaries. *Geophysical Research Letters*, 39(3),
1225 L03602, 2012.
- 1226 Savenije, H.H.G.: A one-dimensional model for salinity intrusion in alluvial estuaries. *Journal of*
1227 *Hydrology*, 85(1-2), 87-109, 1986.
- 1228 Savenije, H.H.G.: Lagrangian solution of St. Venant's equations for alluvial estuary. *Journal of*
1229 *Hydraulic Engineering*, 118(8), 1153-1163, 1992.
- 1230 Savenije, H. H. G. (Ed.): *Salinity and Tides in Alluvial Estuaries*, 1st Edn., Elsevier, Amsterdam, 2005.
- 1231 Savenije, H. H. G. (Ed.): *Salinity and Tides in Alluvial Estuaries*, 2nd Edn., available at:
1232 <http://salinityandtides.com> (last access: 8 March 2015), 2012.
- 1233 Seitzinger, S. P., Harrison, J. A., Dumont, E., Beusen, A. H. W., and Bouwman, A. F.: Sources and
1234 delivery of carbon, nitrogen, and phosphorus to the coastal zone: An overview of Global
1235 Nutrient Export from Watersheds (NEWS) models and their application, *Global Biogeochem.*
1236 *Cycles*, 19, GB4S01, doi:10.1029/2005GB002606, 2005.
- 1237 Schwarz, G.E., Hoos, A.B., Alexander, R.B., and Smith, R.A.: The SPARROW Surface Water-Quality
1238 Model: Theory, Application and User Documentation. U.S. Geological Survey, Techniques
1239 and Methods Report, Book 6, Chapter B3, Reston, Virginia, 2006
- 1240 Sharp, J. H., Yoshiyama, K., Parker, Schwartz, M. C., Curless, S. E., Beauregard, A. Y., Ossolinski, J. E.,
1241 and Davis, A. R.: A Biogeochemical View of Estuarine Eutrophication: Seasonal and Spatial
1242 Trends and Correlations in the Delaware Estuary. *Estuaries and Coasts*, 32, 1023-1043.,
1243 doi:10.1007/s12237-009-9210-8, 2009.
- 1244 Sharp, J. H.: Estuarine oxygen dynamics: What can we learn about hypoxia from long-time records in
1245 the Delaware Estuary? *Limnol. Oceanogr.*, 55(2), 2010, 535–548, 2010.
- 1246 Shih, J.-S., Alexander, R.B., Smith, R.A., Boyer, E.W., Schwarz, G.E., and Chung, S.: An initial SPARROW
1247 model of land use and in-stream controls on total organic carbon in streams of the
1248 conterminous United States, U. S. Geological Survey, Reston, Virginia, 2010.
- 1249 Signorini, S.R., Mannino, A., Najjar Jr, R.G., Friedrichs, M.A.M., Cai, W.J., Salisbury, J., Wang, Z.A.,
1250 Thomas, H., and Shadwick, E.: Surface ocean pCO₂ seasonality and sea-air CO₂ flux
1251 estimates for the North American east coast. *Journal of Geophysical Research C: Oceans*,
1252 118(10), 5439-5460, 2013.
- 1253 Simmons, H. B.: Some effects of inland discharge on estuarine hydraulics, *Proc. Am. Soc. Civ. Eng.-*
1254 *ASCE*, 81, 792, 1955.
- 1255 Soetaert, K., and Herman, P.M.J.: Nitrogen dynamics in the Westerschelde estuary (SW Netherlands)
1256 estimated by means of the ecosystem model MOSES. *Hydrobiologia*, 311(1-3), 225-246,
1257 1995.
- 1258 Stets, E.G., and Strieg, R.G.: Carbon export by rivers draining the conterminous united states. *Inland*
1259 *Waters*, 2(4), 177-184, 2012.
- 1260 Stigter, C., and Siemons, J.: Calculation of longitudinal salt distribution in estuaries as function of
1261 time, Publication Delft Hydraulics Laboratory, 52, The Netherlands, 1967.
- 1262 Thieu, V., Mayorga, E., Billen, G., and Garnier, J.: Subregional and downscaled global scenarios of
1263 nutrient transfer in river basins: Seine-Somme-Scheldt case study. *Global Biogeochemical*
1264 *Cycles*, 24(2) , 2010.
- 1265 Tian, H., Chen, G., Liu, M., Zhang, C., Sun, G., Lu, C., Xu, X., Ren, W., Pan, S., and Chappelka, A.: Model
1266 estimates of net primary productivity, evapotranspiration, and water use efficiency in the
1267 terrestrial ecosystems of the southern United States during 1895-2007. *Forest Ecology and*
1268 *Management*, 259(7), 1311-1327, 2010.

1269 Tian, H., Chen, G., Zhang, C., Liu, M., Sun, G., Chappelka, A., Ren, W., Xu, X., Lu, C., Pan, S., Chen, H.,
1270 Hui, D., McNulty, S., Lockaby, G., and Vance, E.: Century-Scale Responses of Ecosystem
1271 Carbon Storage and Flux to Multiple Environmental Changes in the Southern United States.
1272 *Ecosystems*, 15(4), 674-694, 2012.

1273 U. S. Fish and Wildlife Service. 2014. National Wetlands Inventory website. U.S. Department of the
1274 Interior, Fish and Wildlife Service, Washington, D.C. <http://www.fws.gov/wetlands/>, last
1275 accessed: February 2015.

1276 Vanderborght, J.P., Wollast, R., Loijens, M., and Regnier, P.: Application of a transport-reaction
1277 model to the estimation of biogas fluxes in the Scheldt Estuary. *Biogeochemistry*, 59(1-2),
1278 207-237, 2002.

1279 Vanderborght, J.P., Folmer, I., Aguilera, D.R., Uhrenholdt, T., and Regnier, P.: Reactive-transport
1280 modelling of a river-estuarine-coastal zone system: application to the Scheldt estuary. *Mar.*
1281 *Chem.* 106, 92-110, 2007.

1282 Van der Burgh, P.: Ontwikkeling van een methode voor het voorspellen van zoutverdelingen in
1283 estuaria, kanalen and zeeen, Rijkswaterstaat Rapport, The Netherlands, 1972.

1284 Volta, C., Arndt, S., Savenije, H.H.G., Laruelle, G.G., and Regnier, P.: C-GEM (v 1.0): a new, cost-
1285 efficient biogeochemical model for estuaries and its application to a funnel-shaped system.
1286 *Geosci. Model Dev.*, 7, 1271-1295, doi:10.5194/gmd-7-1271-2014, 2014.

1287 Volta, C., Laruelle, G. G., and Regnier, P.: Regional carbon and CO₂ budgets of North Sea tidal
1288 estuaries, *Estuarine, Coastal and Shelf Science*, 176, 76-90, 2016a.

1289 Volta, C., Laruelle, G. G., Arndt, S., and Regnier, P.: Linking biogeochemistry to hydro-geometrical
1290 variability in tidal estuaries: a generic modeling approach, *Hydrol. Earth Syst. Sci.*, 20, 991-
1291 1030, doi:10.5194/hess-20-991-2016, 2016b.

1292 Vörösmarty, C.J., Fekete, B., and Tucker, B.A.: River Discharge Database, Version 1.0 (RivDIS v1.0),
1293 Volumes 0 through 6. A contribution to IHP-V Theme 1. Technical Documents in Hydrology
1294 Series. UNESCO, Paris, 1996.

1295 Wang, Z.A., and Cai, W.J.: Carbon dioxide degassing and inorganic carbon export from a marsh-
1296 dominated estuary (the Duplin River): A marsh CO₂ pump. *Limnology and Oceanography*,
1297 49(2), 341-354, 2004.

1298

1299 **Table 1:** Estimates of total annual riverine input from watersheds to estuaries (Tg C yr⁻¹). The ranges
 1300 are based on Stets and Striegl (2012), Global NEWS (Mayorga et al. 2010), Hartmann et al. (2009),
 1301 SPARROW (Shih et al. 2010) and DLEM (Tian et al. 2010, 2012). Modified from Najjar et al. 2012.

	DIC	DOC	POC	TOTAL
NAR	0.2-0.8	0.3-2.1	0.1-0.2	0.6-3.1
MAR	1.4-1.8	0.5-2.3	0.1-0.3	2.0-4.4
SAR	0.4-1.4	0.9-1.6	0.1-0.2	1.4-3.2
TOTAL	2.0-4.0	1.7-6.0	0.3-0.7	4.0-10.7

1302

1303

1304

1305 **Table 2:** Published local annually averaged estimates of $\overline{FCO_2}$ in mol C m⁻² yr⁻¹ for estuaries along the
 1306 East coast of the US.”

Name	Lon	Lat	$\overline{FCO_2}$		Reference
			Observed.	Modeled	
Altamaha Sound	-81.3	31.3	32.4	72.7	Jiang et al. (2008)
Bellamy	-70.9	43.2	3.6	3.9	Hunt et al. (2010)
Cocheco	-70.9	43.2	3.1	3.9	Hunt et al. (2010)
Doboy Sound	-81.3	31.4	13.9	25.7	Jiang et al. (2008)
Great Bay	-70.9	43.1	3.6	3.9	Hunt et al. (2011)
Little Bay	-70.9	43.1	2.4	3.9	Hunt et al. (2011)
Oyster Bay	-70.9	43.1	4	3.9	Hunt et al. (2011)
Parker River estuary	-70.8	42.8	1.1	3.9	Raymond and Hopkinson (2003)
Sapelo Sound	-81.3	31.6	13.5	20.6	Jiang et al. (2008)
Satilla River	-81.5	31	42.5	25.7	Cai and Wang (1998)
York River	-76.4	37.2	6.2	8.1	Raymond et al. (2000)
Hudson River	-74	40.6	13.5	15.5	Raymond et al. (1997)
Florida Bay	-80.68	24.96	1.4	n.a.	Dufore (2012)

1307

1308

1309 **Table 3:** State variables and processes explicitly implemented in CGEM.

State variables		
Name	Symbol	Unit
Suspended Particulate Mater	SPM	gL ⁻¹
Total Organic Carbon	TOC	μM C
Nitrate	NO ₃	μM N
Ammonium	NH ₄	μM N
Phosphate	DIP	μM P
Dissolved Oxygen	DO	μM O ₂
Phytoplankton	Phy	μM C
Dissolved Silica	dSi	μM Si
Dissolved Inorganic Carbon	DIC	μM C
Biogeochemical reactions		
Name	Symbol	Unit
Gross primary production	GPP	μM C s ⁻¹
Net primary production	NPP	μM C s ⁻¹
Phytoplankton mortality	M	μM C s ⁻¹
Aerobic degradation	R	μM C s ⁻¹
Denitrification	D	μM C s ⁻¹
Nitrification	N	μM N s ⁻¹
O ₂ exchange with the atmosphere	FO ₂	μM O ₂ s ⁻¹
CO ₂ exchange with the atmosphere	FCO ₂	μM C s ⁻¹
SPM erosion	E _{SPM}	gL ⁻¹ s ⁻¹
SPM deposition	D _{SPM}	gL ⁻¹ s ⁻¹

1310

1311

1312 **Table 4:** Yearly averaged surface area (*S*), fresh water discharge (*Q*), residence time (*Rt*), *FCO₂* and
 1313 *NEM* of all simulated estuaries.

long degrees	lat degrees	<i>S</i> km ²	<i>Q</i> m ³ s ⁻¹	<i>Rt</i> days	$\overline{FCO_2}$ mol C m ⁻² yr ⁻¹	\overline{NEM} mol C m ⁻² yr ⁻¹	<i>FCO₂</i> 10 ⁶ mol C yr ⁻¹	<i>NEM</i> 10 ⁶ mol C yr ⁻¹
NAR								
-67.25	44.75	7	38.5	15	3.7	-37.4	27	-270
-67.25	45.25	12	73.6	15	6.0	-56.7	71	-666
-67.25	45.25	12	73.6	15	13.8	-56.6	162	-666
-67.75	44.75	3	68.5	4	6.7	-63.5	23	-221
-68.25	44.75	14	69.5	19	4.1	-56.2	58	-791
-68.75	44.75	89	309.9	23	27.4	-58.2	2431	-5163
-69.75	44.25	50	626.6	5	32.3	-74.4	1607	-3703
-70.25	43.75	3	25.8	10	2.1	-21.0	7	-71
-70.75	41.75	288	103.6	958	5.0	-4.0	1428	-1146
-70.75	42.25	63	210.7	40	16.2	-32.9	1025	-2081
-70.75	42.75	17	105.8	3	56.3	-69.0	943	-1155
MAR								
-70.75	43.25	31	29.9	11	21.6	-37.4	662	-1146
-71.25	41.75	257	28.2	808	3.9	-2.5	997	-650
-71.75	41.25	21	112.4	4	35.2	-32.6	726	-672
-72.75	40.75	20	25.4	62	30.7	-21.1	623	-430
-72.75	41.25	10	142.5	2	150.8	-36.9	1578	-386
-72.75	41.75	55	476.6	3	55.9	-45.7	3088	-2523
-73.25	40.75	19	26.8	56	31.4	-28.4	608	-550
-74.25	40.75	1192	608.2	126	15.5	-11.8	18432	-14047
-75.25	38.25	399	80.5	172	13.9	-5.0	5558	-2016
-75.25	38.75	354	31.8	357	7.5	-3.0	2659	-1076
-75.25	39.75	1716	499.0	221	10.0	-7.8	17072	-13439
-75.75	39.25	224	18.3	434	7.5	-2.9	1685	-640
-76.25	39.25	3427	717.1	352	8.1	-5.1	27646	-17352
-76.75	37.25	586	272.3	74	15.0	-10.4	8810	-6084
-76.75	37.75	154	36.3	163	10.7	-6.6	1654	-1023
-76.75	39.25	59	71.2	29	48.6	-34.6	2862	-2038
-77.25	38.25	206	30.2	268	6.1	-3.3	1265	-676
-77.25	38.75	568	259.2	118	16.7	-10.8	9488	-6134
SAR								
-78.25	34.25	48	167.4	7	122.5	-62.4	5916	-3015
-79.25	33.25	47	56.3	42	43.4	-36.5	2056	-1728
-79.25	33.75	45	291.4	8	85.1	-78.7	3843	-3551
-79.75	33.25	25	33.8	15	37.9	-32.8	956	-828
-80.25	32.75	25	31.0	50	48.8	-42.5	1214	-1057
-80.25	33.25	92	75.5	61	62.7	-61.2	5769	-5625
-80.75	32.25	71	21.1	182	12.9	-7.0	918	-501
-80.75	32.75	164	63.1	95	20.6	-11.5	3372	-1879
-81.25	31.75	92	71.7	45	25.7	-20.9	2361	-1926
-81.25	32.25	130	379.8	11	51.7	-39.2	6732	-5097
-81.75	30.75	34	18.7	61	17.5	-14.7	602	-505
-81.75	31.25	130	17.7	294	5.5	-4.0	713	-523
-81.75	31.75	56	350.5	4	72.7	-67.4	4068	-3770

1314

1315 **Table 5:** Seasonal contribution to FCO_2 and NEM in each the sub-region. The seasons displaying the
 1316 highest percentages are indicated in bold. Winter is defined as January, February and March, Spring
 1317 as April, May and June and so on...

Region	NEM mol C y ⁻¹	winter %	spring %	summer %	fall %	FCO_2 mol C y ⁻¹	winter %	spring %	summer %	fall %
NAR	-16.3 10 ⁹	14.7	21.2	37.0	27.2	7.2 10 ⁹	26.3	18.9	26.5	28.3
MAR	-72.2 10 ⁹	21.9	25.9	28.8	23.4	108.3 10 ⁹	29.8	23.3	20.7	26.2
SAR	-30.5 10 ⁹	24.6	20.9	30.3	24.2	39.2 10 ⁹	26	23.4	27	23.6

1318

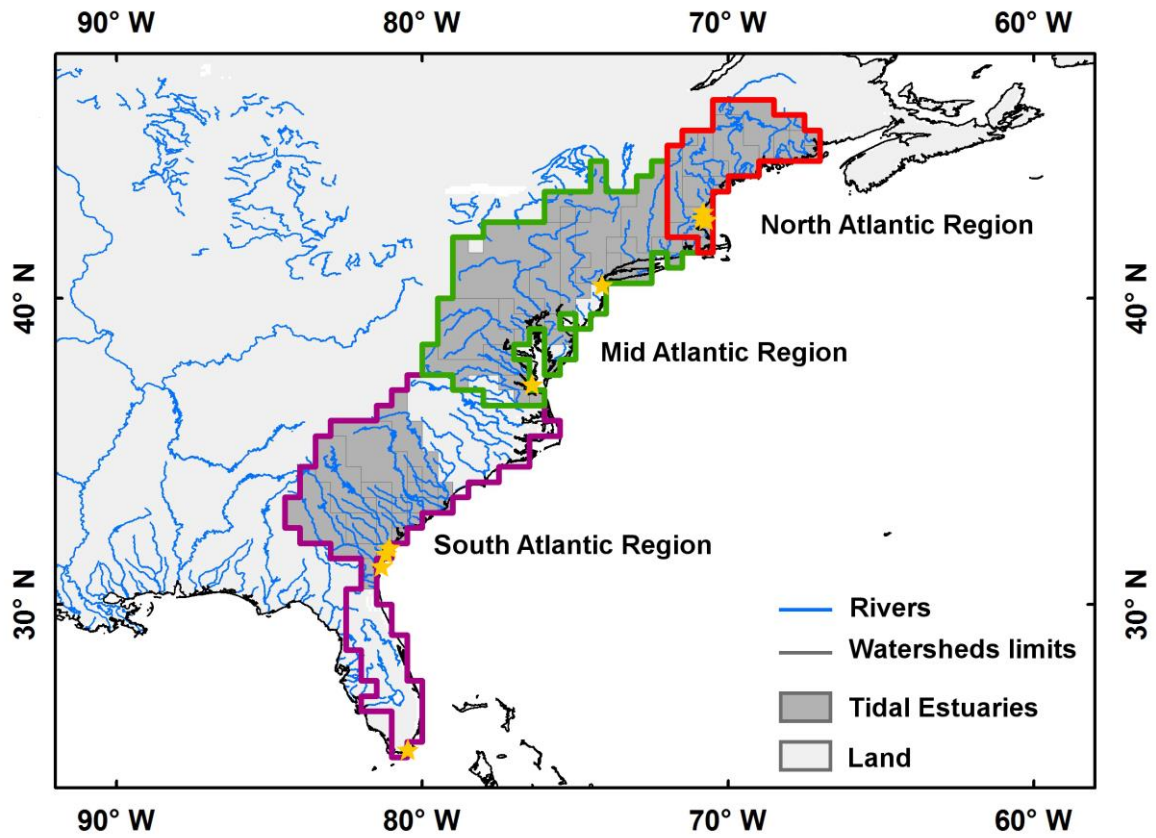
1319

1320 **Table 6:** Regressions and associated coefficient of determination between the depth normalized
 1321 residence time (S/Q) and $-\overline{NEM}/f(T)$, $\overline{FCO_2}/f(T)$ and $CFilt$.

Region	$-\overline{NEM}/f(T)$	$\overline{FCO_2}/f(T)$	$CFilt$
NAR	$y = 27.84 x^{-0.17}$ $r^2 = 0.11$	$y = 6.07 x^{0.00}$ $r^2 = 0.00$	$y = 15.08 \log_{10}(x) + 4.86$ $r^2 = 0.40$
MAR	$y = 26.03 x^{-0.63}$ $r^2 = 0.86$	$y = 34.36 x^{-0.58}$ $r^2 = 0.68$	$y = 40.46 \log_{10}(x) + 9.60$ $r^2 = 0.70$
SAR	$y = 28.36 x^{-0.71}$ $r^2 = 0.76$	$y = 32.82 x^{-0.66}$ $r^2 = 0.80$	$y = 23.19 \log_{10}(x) + 43.71$ $r^2 = 0.46$
MAR + SAR	$y = 25.85 x^{-0.64}$ $r^2 = 0.82$	$y = 31.64 x^{-0.58}$ $r^2 = 0.70$	$y = 33.30 \log_{10}(x) + 24.88$ $r^2 = 0.57$
NAR + MAR + SAR	$y = 28.98 x^{-0.66}$ $r^2 = 0.82$	$y = 12.98 x^{-0.33}$ $r^2 = 0.30$	$y = 40.64 \log_{10}(x) + 11.84$ $r^2 = 0.70$

1322

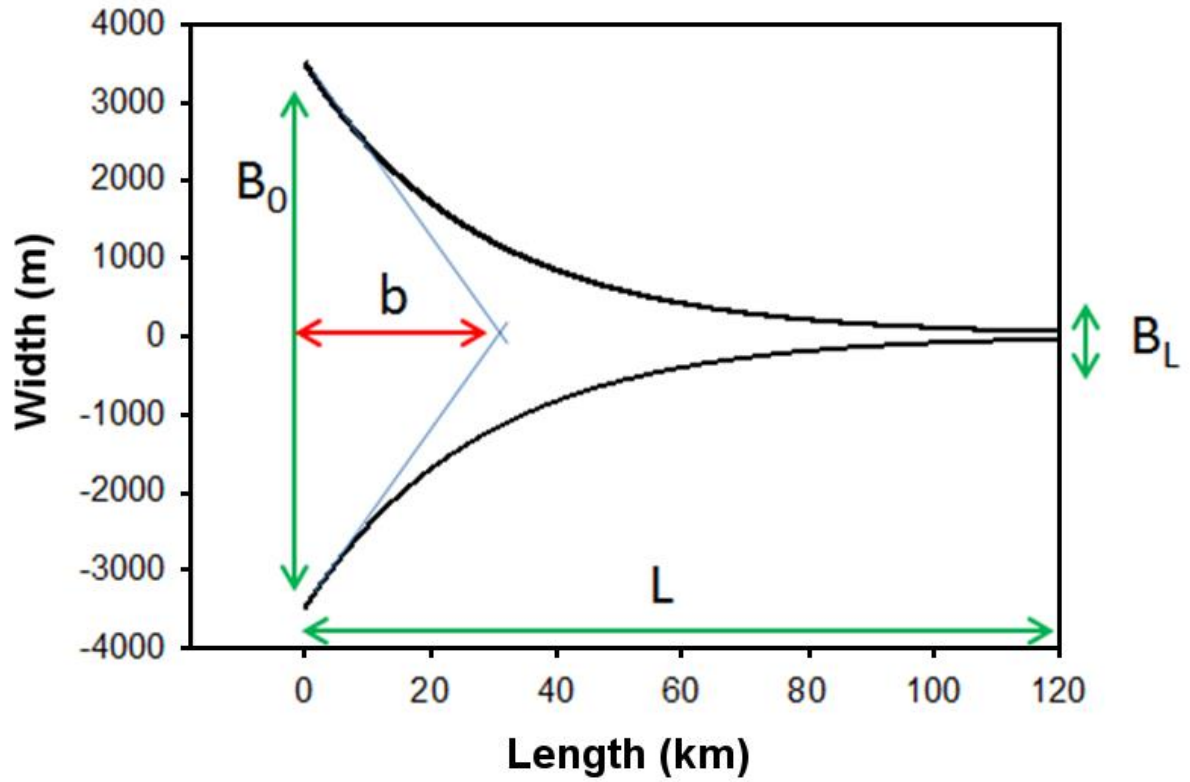
1323



1324

1325 **Figure 1:** Limits of the 0.5 degrees resolution watersheds corresponding to tidal estuaries of the East
 1326 coast of the US. 3 sub-regions are delimited with colors and orange stars represent the location of
 1327 previous studies.

1328

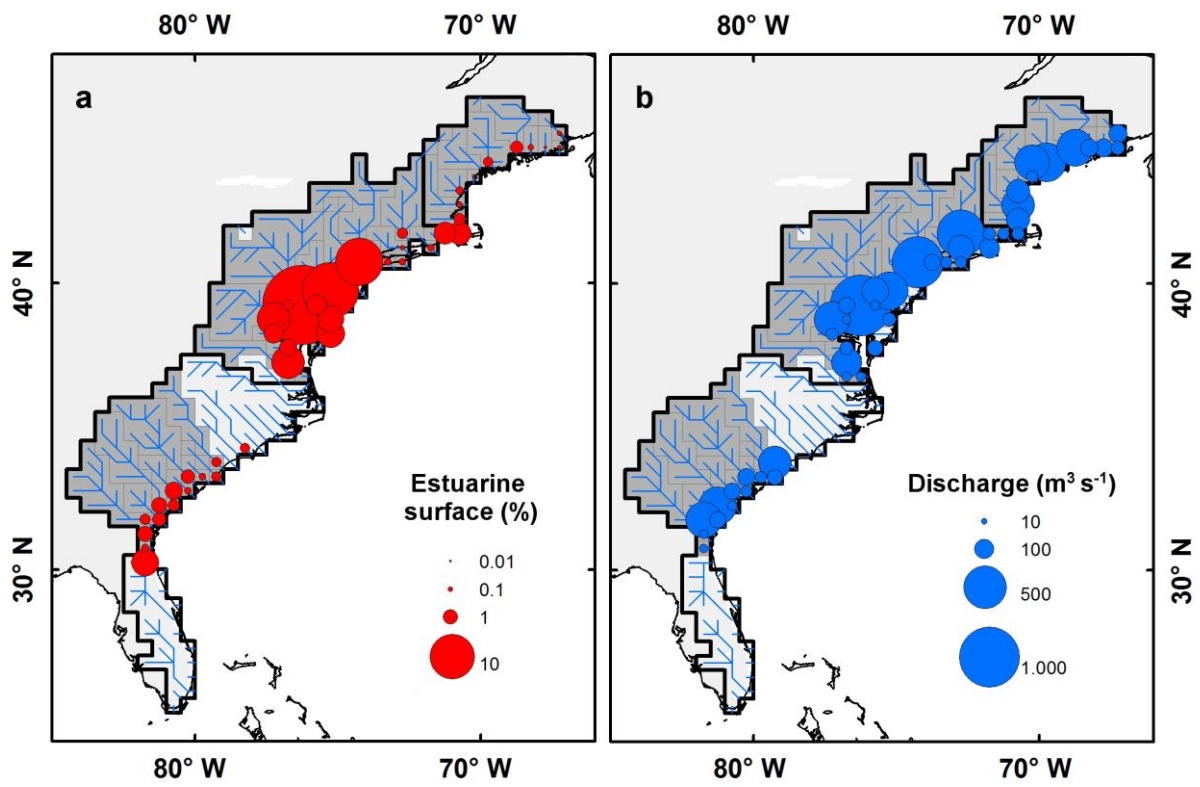


1329

1330 **Figure 2:** Idealized estuarine geometry and main parameters. Parameters indicated by green arrows
 1331 are measured, b is calculated. See section 2.3.1 for further details.

1332

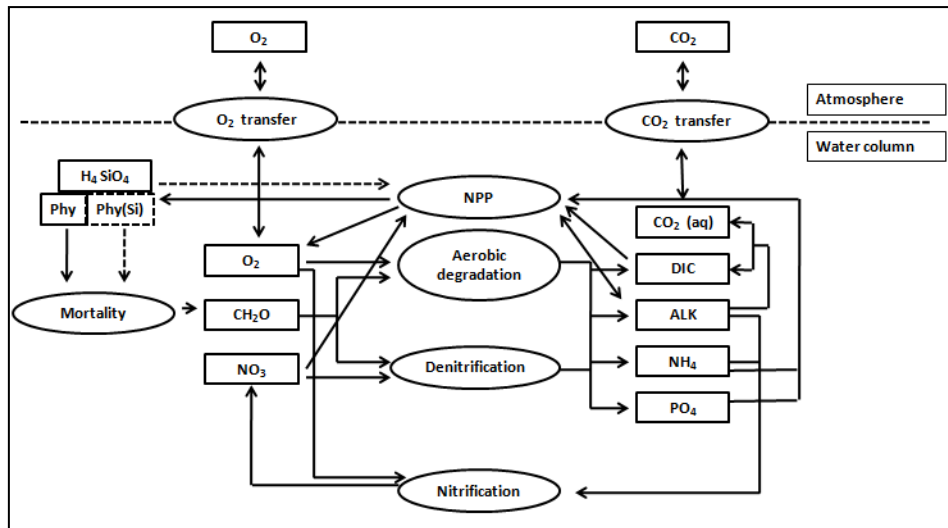
1333



1334

1335 **Figure 3:** Estuarine surface area (a) and mean annual freshwater discharge (b) for each tidal estuary
1336 of the East coast of the US. Estuarine surface area are expressed as percentage of the entire surface
1337 area of the region (19830 km²)

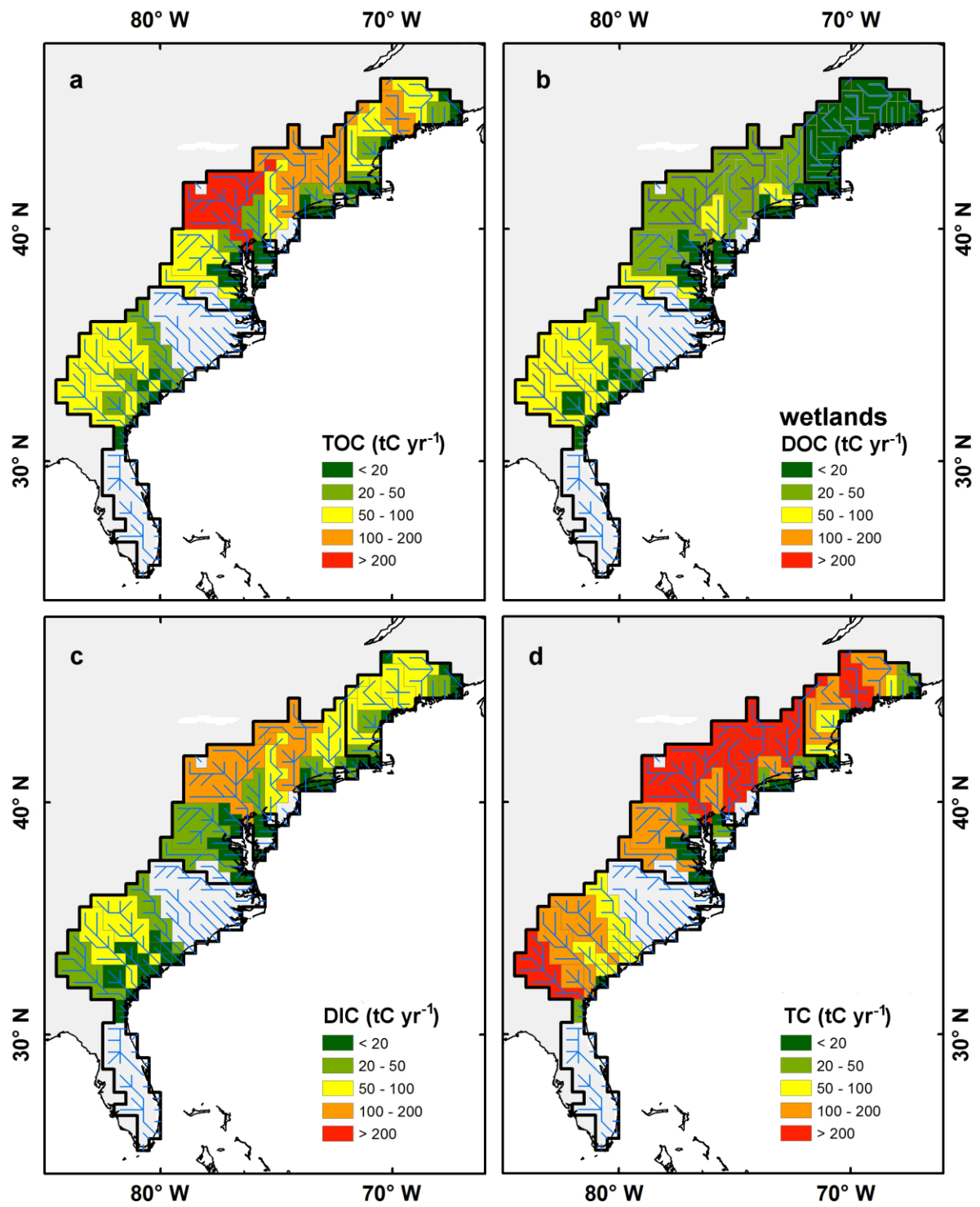
1338



1339

1340 **Figure 4:** Conceptual scheme of the biogeochemical module of C-GEM used in this study. State-
 1341 variables and processes are represented by boxes and oval shapes, respectively. Modified from Volta
 1342 et al., 2014.

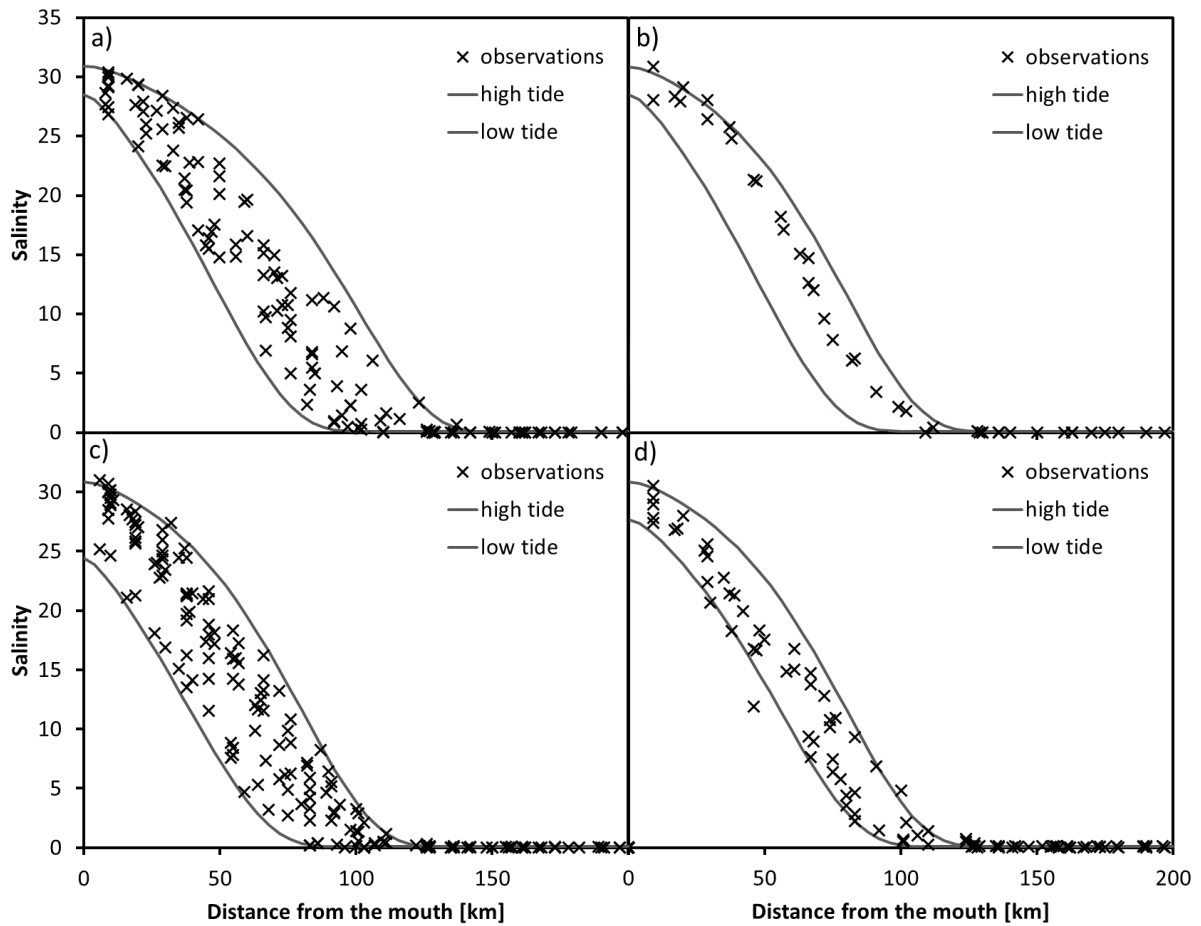
1343



1344

1345 **Figure 5:** Annual river carbon loads of TOC (a), annual DOC fluxes from wetlands (b), annual river
 1346 carbon loads of DIC (c) and annual TC fluxes (d). All fluxes are indicated per watershed.

1347

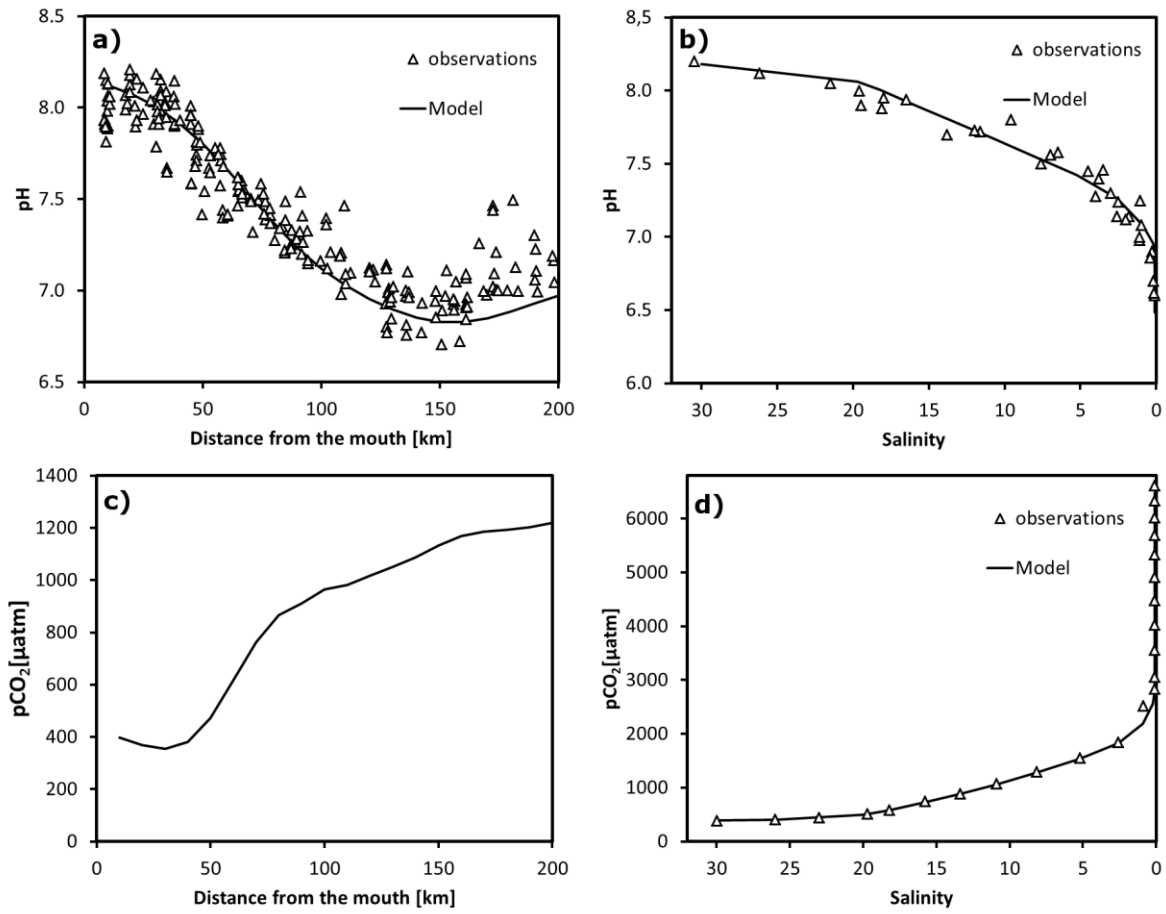


1348

1349 **Figure 6.** Modeled (lines) and measured (crosses) salinities in the Delaware Bay estuary for January

1350 (a), February (b), May (c), June (d). The two lines correspond to high and low tides.

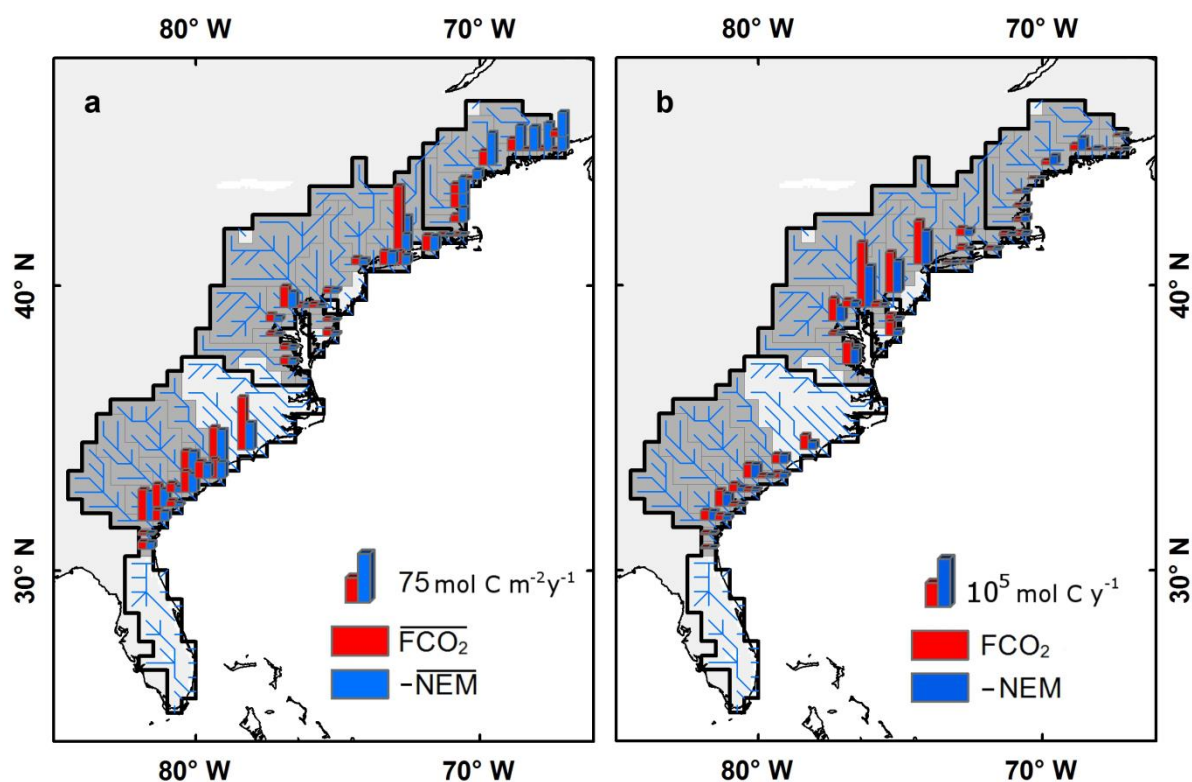
1351



1352

1353 **Figure 7.** Longitudinal profiles of pH (top) and pCO₂ (bottom) for the Delaware Bay (left) and
 1354 Altamaha river estuary (right).

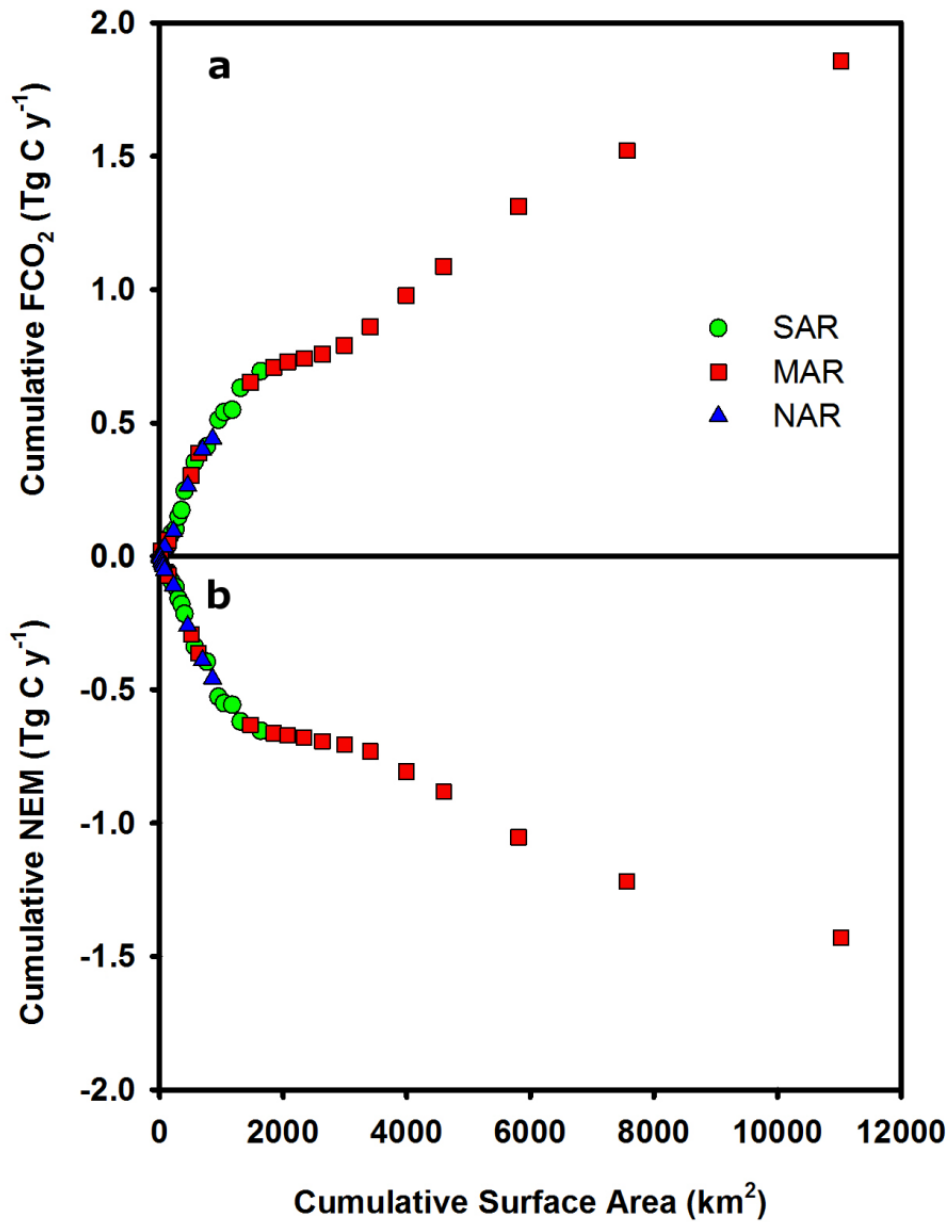
1355



1357

1358 **Figure 8:** Spatial distribution of spatially averaged value (a) and integrated value (b) of mean annual
 1359 FCO_2 (red) and $-NEM$ (blue) along the East coast of the US. On panel a, the notation with overbars
 1360 ($\overline{FCO_2}$ and $\overline{-NEM}$) represents rates per unit surface. For the sake of the comparison with $\overline{FCO_2}$, Fig.
 1361 8 displays $\overline{-NEM}$ because the model predicts that all estuaries in this region are net heterotrophic.

1362

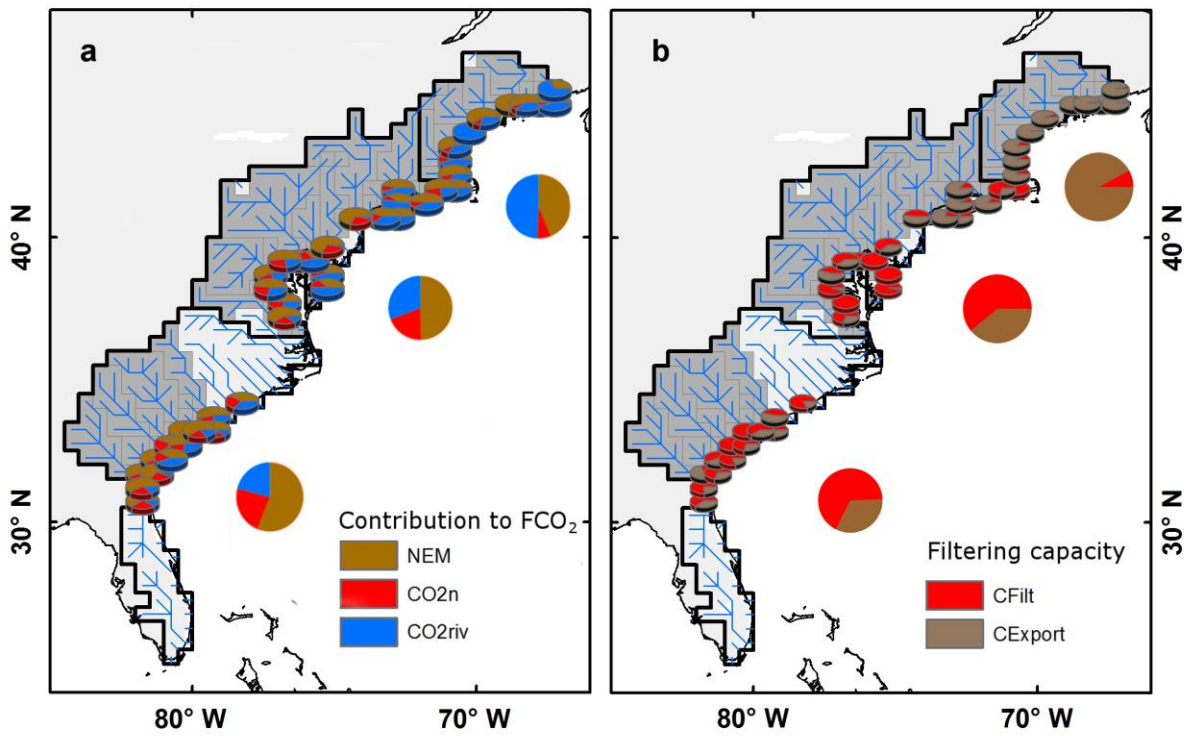


1363

1364 **Figure 9:** The Cumulative FCO_2 (a) and NEM (b) as functions of the cumulative estuarine surface area.

1365 Systems are sorted by increasing surface area.

1366

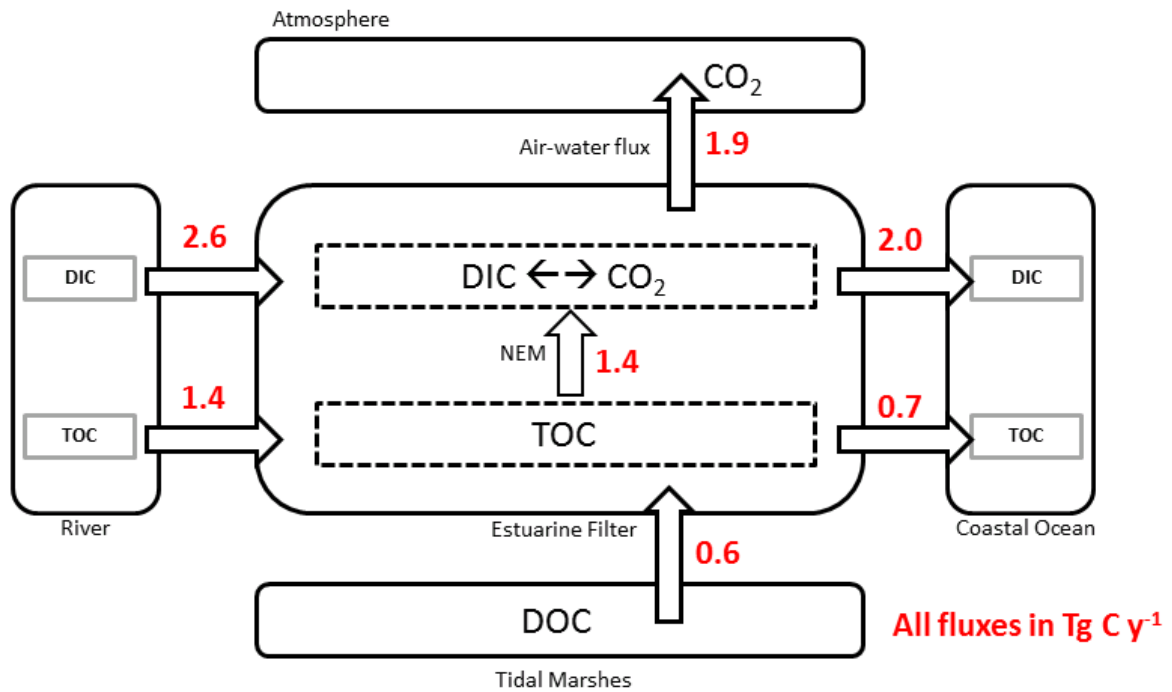


1367

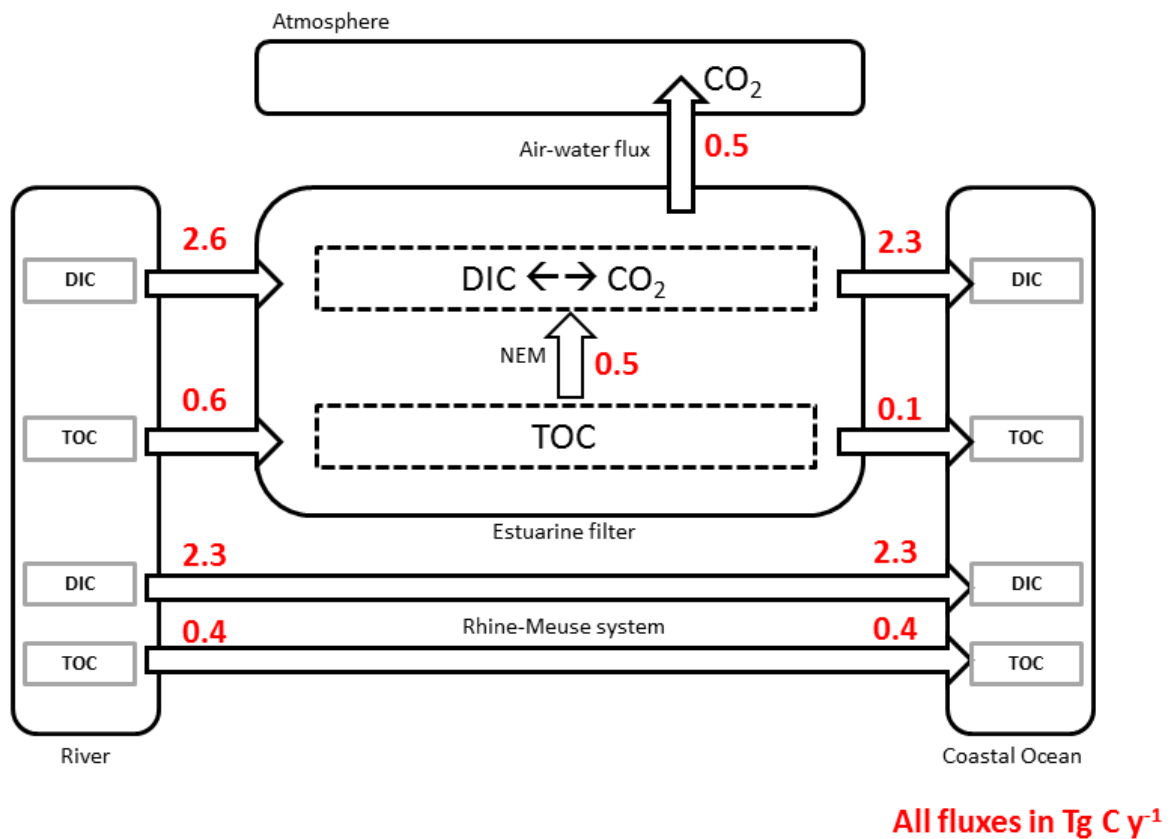
1368 **Figure 10:** Contribution of *NEM*, nitrification and riverine waters super-saturated waters to the mean
 1369 annual FCO_2 (a). Spatial distribution of mean annual carbon filtration capacities ($CFilt$) and export
 1370 ($CExport$) along the East coast of the US (b).

1371

a) Eastern US coast

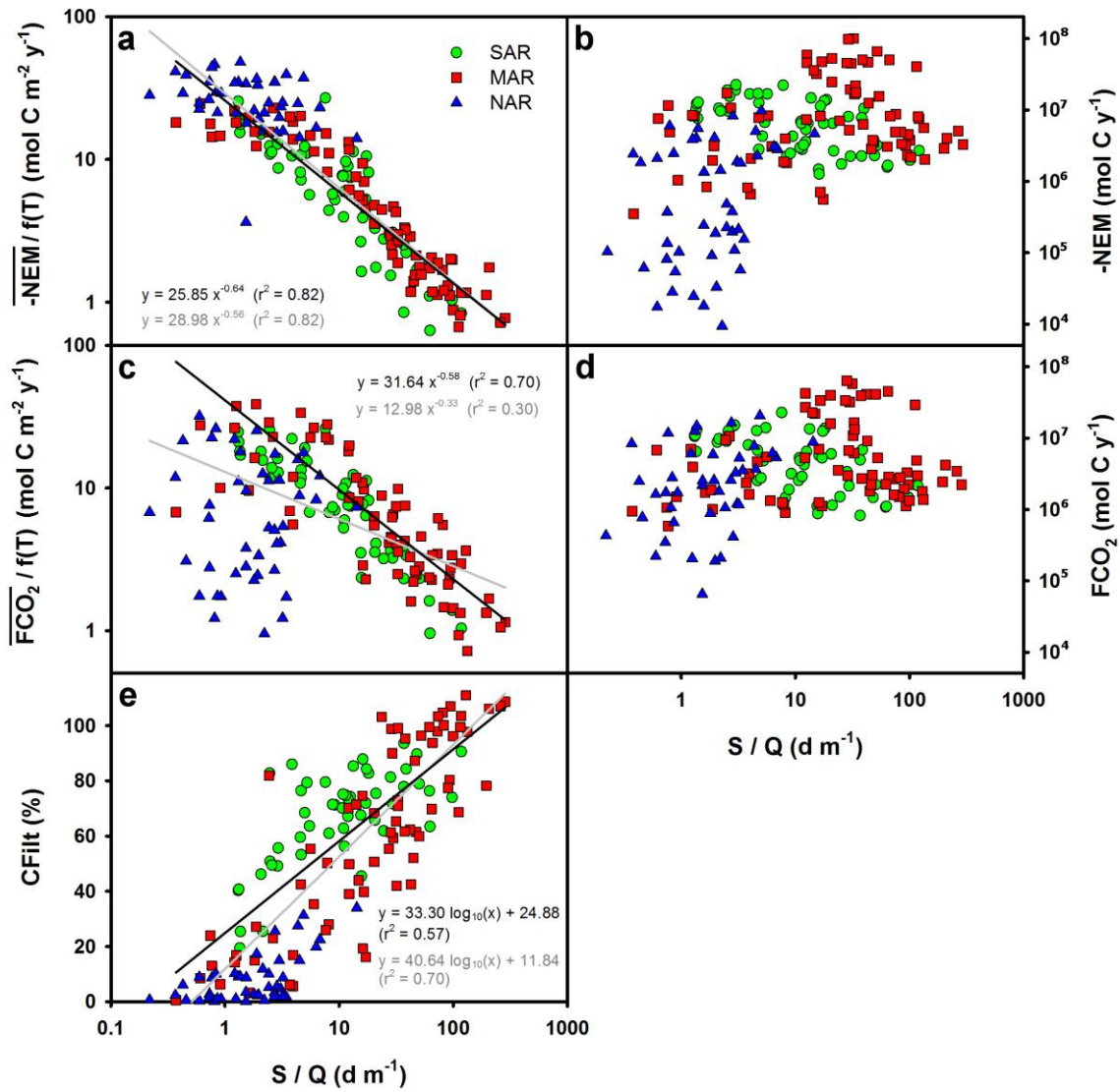


b) North Sea coast



1372

1373 **Figure 11:** Annual carbon budget of the estuaries of the East coast of the US (a) and of the coast of
 1374 the North Sea (b, modified from Volta et al., 2016a).



1375

1376 **Figure 12:** System scale integrated biogeochemical indicators expressed as functions of the depth
 1377 normalized residence time expressed as the ratio of the estuarine surface S and the river discharge Q
 1378 for all seasons. Panels b, d and e represent NEM, $-FCO_2$ and CFilt, respectively. Panels a and c
 1379 represent NEM, $-FCO_2$ normalized by a temperature Q_{10} function. Black lines are the best fitted linear
 1380 regressions obtained using all the point. Grey lines are best fit using only the estuaries from the MAR
 1381 and SAR regions.

1382